12-1997

Breast Cancer Mass Detection using Difference of Gaussians and Pulse Coupled Neural Networks

Donald A. Cournoyer

AFIT/GE/ENG/97D-07

BREAST CANCER MASS DETECTION USING DIFFERENCE OF GAUSSIANS AND PULSE COUPLED NEURAL NETWORKS

THESIS

Donald A. Cournoyer
1st Lieutenant, USAF

AFIT/GE/ENG/97D-07

Approved for public release; distribution unlimited

The views expressed in this thesis are those of the author and do not reflect the official policy or position of the Department of Defense or the United States Government.

AFIT/GE/ENG/97D-07

Breast Cancer Mass Detection
Using Difference of Gaussians and Pulse Coupled Neural Networks

THESIS

Presented to the Faculty of the Graduate School of Engineering

of the Air Force Institute of Technology

Air University

In Partial Fulfillment of the

Requirements for the Degree of

Master of Science in Electrical Engineering

Donald A. Cournoyer, B.S. Electrical Engineering

1st Lieutenant, USAF

December, 1997

AFIT/GE/ENG/97D-07

Breast Cancer Mass Detection
Using Difference of Gaussians and Pulse Coupled Neural Networks

Donald A. Cournoyer, B.S. Electrical Engineering

1st Lieutenant, USAF

Approved:

[redacted]

Dr. Martin P. DeSimio
Thesis Advisor

6 Nov 97
Date

[redacted]

Dr. Steven K. Rogers
Committee Member

6Nov97
Date

[redacted]

Dr. Matthew Kabrisky
Committee Member

6 NOV 97
Date

Acknowledgements

I dedicate this research to my wife, Kim, and two daughters, Courtney and Rachel. You were constantly on my mind during each and every hour I was slaving away on this research. Without your inspiration I would have never found the motivation necessary to succeeed. Thank you for making every moment away from work an enjoyable one.

My appreciations are extended to a number of people who made this research possible. I would not have experienced these successes without the efforts of my advisor, Dr. Marty DeSimio, who focused and energized my research, and my committee members, Dr. Steve Rogers and Dr. Matt Kabrisky, who provided incredible insight and motivation. I thank my sponsor, Maj. Jeff Hoffmeister, M.D., who provided invaluable input from a medical perspective. I also would like to thank the entire AFIT Breast Cancer Group, especially Capt. Eddie Ochoa, who introduced me to the world of CAD breast cancer research; Capt. Randy Broussard, who provided PCNN expertise; Capt. Tom Rathbun, who supplied GA expertise; Maj. Kevin Lee and Maj. Rick Raines, who provided enlightening suggestions; and Shaun Stapleton and Jill Leighner, who provided research support.

Last, I would like to thank the members of the Comm Lab for always keeping things light-hearted, even in the most frustrating moments during this research effort.

Donald A. Cournoyer

Table of Contents

List of Figures

List of Tables

Abstract

Breast cancer will kill an estimated 43,900 women in the United States in 1997. Another 180,200 women will be newly diagnosed with breast cancer in 1997. Breast cancer has been calculated to have the potential of striking one in eight women based on a longevity of 95 years. Mammography is currently the best method for detecting breast cancer. However, a significant portion, 10 to 30 percent, of women with breast cancer have negative mammograms. Two-thirds of these false-negative mammograms prove to be evident in retrospect. Having a second radiologist perform a second reading has proven to be successful at correctly diagnosing breast cancer.A lower cost and more reliable alternative is a computer system to perform the second reading.

One indicator of breast cancer is a mass or density. This thesis will develop a new algorithm to identify masses in mammograms. The system developed for this thesis is capable of assisting a radiologist in making decisions.

The database used for algorithm development consisted of 104 mammograms selected from cases at the Wright-Patterson Air Force Base Hospital. These mammograms contain 108 masses. The mammograms were digitized to 100 μm resolution with 12 bits of gray-scale and cropped to create 2048 x 1024 pixel images.

The mass detection system consists of several modules. The digitized mammogram is decimated to a 512 x 256 image, preprocessed for easier detection, and filtered with a Difference of Gaussians filter. The system then detects objects with mass characteristics using a Pulse Coupled Neural Network, extracts morphological and textural features from each possible detection, and classifies as mass or normal tissue. The detection module of the system detects 89 percent of the 108 masses, 96.36 percent of the cases, with a FP rate of 11.37 per image. The classifier eliminates 4.67 FPs per image while retaining 92.7 percent of the detected masses. On a 2-view per case basis, the system successfully detects and classifies 94.55 percent of masses with 13.4 FPs per case.

Breast Cancer Mass Detection

Using Difference of Gaussians and Pulse Coupled Neural Networks

I. Introduction

1.1 Background

Breast cancer will kill an estimated 43,900 women in the United States in 1997 (46). Another 180,200 women will be newly diagnosed with breast cancer in 1997 (46). Breast cancer is the second leading cause of cancer death in women, exceeded only by lung cancer (46). It is the leading cause of cancer death among women aged 40 to 55. Breast cancer has been calculated to have the potential of striking one in eight women based on a longevity of 95 years (44).

Mammography is the use of x-ray technology to examine the internal structure of breasts. The purpose of mammograms is to find abnormalities in the breast that are too small to see or feel by external exam. If a tumor is found in this small stage, the survival rate is very significantly improved (45). Mammography is currently the best method for detecting breast cancer. However, a significant portion, 10 to 30 percent, of women with breast cancer have negative mammograms (13). Two-thirds of these false-negative mammograms prove to be evident in retrospect (13). These missed detections can be attributed to the subtle nature of radiographic findings, poor image quality, eye fatigue, or oversight by the radiologist (13). Although some lesions are missed, most recent data indicates that death rates have begun to decline (46). Most of this apparent decrease is believed to be a result of marked increases in the use of mammography, providing better detection of early-stage breast cancers (46). Early detection improves the chance that breast cancer can be located, diagnosed, and treated successfully.

1.2 Second Readings

Although mammography is the leading method of detection, mistakes occur and women die. Having a second radiologist perform a second reading has proven to be suc-

cessful at correctly diagnosing breast cancer (2, 48). Dr. Byrd performed double readings over a 3 year period (2). During that time, 11 of 208 total cancers were missed by the first reader, but were identified by virtue of the second radiologist. In another study, two experienced radiologists screened 18,827 women independently (48). Of these women, 90 total lesions were detected in retrospect. During the study, the screeners identified 70 and 62 tumors respectively (48). However, 10 extra cancerous detections were detected by using two screeners (48). Fifteen percent more breast cancer cases were detected, because of double readings (48). The conclusions of the studies strongly suggest that double readings should have a high priority in a screening program and be performed whenever feasible (2, 48).

Mammography has become a high-volume x-ray procedure causing radiologists to be consumed by the overwhelming workload (13). Employing twice as many radiologists could double the expense of mammography, which, therefore, isn't an option. A lower cost and more reliable alternative is a computer system to perform the second reading (13).

1.3 Computer-Aided Diagnosis

Computer-aided diagnosis (CAD) is when a radiologist uses the results of a computerized analysis of radiographic images to assist in detecting lesions and in making diagnostic decisions (13). The aim of CAD is to aid radiologists by increasing the number of detections while reducing the number of false-positive diagnoses of malignancy, thereby decreasing patient morbidity, as well as the number of surgical biopsies performed and their associated complications (13). The measure of the success of CAD detection schemes is the performance of radiologists when the computer output is used as an aid as compared with the performance of radiologists alone (13).

Kegelmeyer performed a study of the success of CAD as a second reader (23). The study involved four radiologists, who at different times, reviewed 85 cases twice, once with and once without computer assistance. CAD increased the average radiologist sensitivity, percent of true positives located, by 9.7 percent, moving from 80.6 to 90.3 percent with no decrease in average specificity, percent of falsely classified benign cases (23).

1.4 Problem Statement

CAD, serving as a second reader, has been shown to improve the success of radiologists at detecting breast cancer. This thesis will develop a new algorithm to identify masses in mammograms. The system developed for this thesis will be capable of assisting a radiologist in making decisions.

1.5 Scope

The system developed for this research detects masses in mammograms using a single image. The research does not include microcalcification or parenchymal pattern detection, but could be modified to work in conjunction with such systems. The basis of any CAD system is to maintain the current practice of having the radiologist make the final decision on patient case management.

The database used for algorithm development consisted of 104 mammograms with 108 masses selected from cases at the Wright-Patterson Air Force Base Hospital. The mammograms were digitized to 100 micron resolution with 12 bits of gray-scale and cropped to create 2048 x 1024 pixel images. The information contained in these images was manipulated using Matlab and C++ code to develop an optimized system for the detection of masses in radiographic mammograms for use as a second reading.

1.6 Overview

The remainder of this thesis is organized as follows: Chapter II provides background on breast cancer and mass research. Chapter III explains the methodology of the system. Chapter IV presents the results and analyzes the performance of the system. Conclusions are presented in Chapter V. The appendix contains detailed information about the database and results.

II. Background

2.1 Breast Cancer

Breasts are composed of ligaments, glands, ducts, and fatty tissue (7). Breast cancer is the result of abnormal growth of cells in the breast (26). Three indicators radiologists look for as signs of cancers are calcification, parenchymal patterns, and masses. After these indicators are identified, the radiologist makes a decision on patient management, including follow-ups and biopsies, to determine malignancy (13).

2.1.1 Calcifications. Calcifications, or microcalcifications, are mammographically detectable, naturally occurring calcium deposits, which appear at the highest intensity levels of mammograms. Microcalcifications range in size from 0.1 to 0.3 mm in diameters and appear circular in shape. Microcalcifications are considered to be associated with cancer when they are grouped together and have pointed edges. Microcalcification detection has been the subject of much CAD research at AFIT (10, 25, 31, 36). These methods identified microcalcifications from their surroundings by filtering, adaptive thresholding, or texture analysis.

2.1.2 Parenchymal Patterns. Parenchymal patterns are the textural patterns which make up the breast (13). Wolfe classifies four risk groups based on four grades for developing carcinoma of the breast (49). Tahoces *et al* uses a method containing Fourier transforms, local-contrast analysis, and gray-level distribution and quantification to classify mammograms into one of Wolfe's four patterns. Based on this quantitative texture measure, radiologist could assess the patients risk for developing breast carcinoma (47).

2.1.3 Masses. The word "mass" is used to indicate that a three-dimensional lesion can be located in multiple views of mammograms. Otherwise, a lesion seen in only one view is termed a density. In this thesis, the term "mass" is used to label detections even when it has been located in only one view, since only one image at a time is being used for experimentation. Examples of tissues, frequently confused with masses, are glands, ducts, and dense portions of the breast (27). Since masses can be obscured or simulated

by these normal parenchymal tissues, interpretation can be difficult for both computers and humans (14, 42).

Masses can vary in diameter from less than 0.5 cm to over 5 cm (29, 35). Masses typically become palpable at sizes even less than 2 cm in diameter (38). Typically, mass regions in mammograms are characterized by being 1) brighter than surrounding tissue, although not as high contrast as microcalcifications, 2) having uniform density inside the lesion, 3) approximately circular in shape, and 4) fuzzy around its edges (27).

Locating suspicious areas in mammograms is difficult since small differences in density between normal and tumorous tissues create low contrast between a tumor area and its background (27). The boundaries can appear fuzzy, or possibly only partially visible (27). Subtle masses can contain edges of low signal-to-noise ratio and complicated structured background (37).

Two specific types of tumors being investigated in CAD are stellate and circumscribed lesions (34). Stellate lesions consist of a central tumor surrounded by radial spicules (34). Circumscribed lesions appear nearly circular and have a fuzzy boundary (34).

2.1.4 Utility of CAD. Computers perform various functions of image analysis differently than humans and have potential to complement human observers (14). Thus, the interpretation of mammograms may benefit from computer assistance by directing radiologists to suspect regions, in order to avoid simple oversight. Computers extract features from mammograms to classify areas that may need to be further investigated. Depending on their nature, these features may or may not be visible to a radiologist (14).

The benefit of using computer-extracted features is the objectivity and reproducibility of the results. Radiologists, however, use many radiographic image features, which they extract and interpret simultaneously and instantaneously. The development of computer-extracted features requires initial determination of which individual features are clinically significant prior to developing means for their extraction. The interpretation of screening mammograms lends itself to CAD, because of the repetitive task involving mostly normal images (14). The aim of CAD is to alert the radiologist to structures that might be otherwise overlooked.

2.2 CAD Mass Research

The computer is capable of detecting objects based on characteristics such as circularity, size, contrast from surroundings, and textures. Research groups have developed various methods for finding masses and diagnosing malignancy.

2.2.1 Multiple View Schemes. Although radiologists use many mammograms portraying multiple views over many years, CAD detection schemes use either one or two views in making their evaluation. Yin *et al* use a nonlinear bilateral subtraction technique to locate assymetric density patterns in corresponding portions of right and left breasts (50). False positive (FP) reduction is accomplished through analysis of the area, contrast, circularity, and border-distance based on the density and geometry of the masses (50).

Zheng *et al* investigate the advantages and disadvantages of using the bilateral subtraction method versus a Gaussian filter method operating on a single image (51). Their single image segmentation scheme yields more suspicious regions than their bilateral-image subtraction scheme both prior and after feature analysis (51). The two reasons for a bilateral subtraction scheme to lose true positive (TP) regions are: 1) the undetected masses are generally small and of low contrast occurring anywhere in the image, or 2) they are close to skin boundaries, where alignment and scaling between paired images are generally difficult (51).

2.2.2 Single View Methods. The following methods address mass detection using a single image. Unless otherwise specified, the schemes are designed to work on both circumscribed and stellate lesions.

Petrick *et al* use a mass segmentation procedure involving an adaptive density-weighted contrast enhancement (DWCE) filter in conjunction with Laplacian-Gaussian edge detection (37).The DWCE filter enhances structures within the breast followed by a simple edge detector which defines the boundaries of the objects. An object splitting technique is used to eliminate tails from detections. Morphological features are then extracted and used for classification.

Li *et al* employ adaptive thresholding and a multi-resolution Markov Random Field (MRF) model-based method to segment suspicious regions of interest (ROIs) (29). This process begins by decimating the digitized mammograms to obtain multiple resolutions. Initial segmentation of the lowest resolution image is performed by adaptive thresholding. By iteratively analyzing a varying number of a pixel's neighbors, a pixel is classified as background, normal tissue, or suspicious tissue. Once pixels are no longer significantly changing classifications, the resolution is increased. Segmentation is complete when the highest resolution image has been completely classified.

Ng and Bischof apply edge-oriented, field-oriented, and spine-oriented approaches to detect lesions (34). Kaewlium and Longbotham use the correlation of three spatially separated Gabor functions convolved with a digitized mammogram to highlight masses and parenchymal patterns (20).

Chan *et al* use texture features derived from spatial gray level dependence matrices to differentiate masses and normal breast tissue (8). Working on 256 x 256 ROIs, five texture features were found important for classification based on stepwise linear discriminant analysis. These features are derived from an original eight features of correlation, entropy, energy (angular second moment), inertia, inverse difference moment, sum average, sum entropy, and difference entropy.

Lai *et al* detect circumscribed masses with a method using a modified median filter to enhance mammogram images and template matching to detect breast tumors (27). The template matching stage locates suspicious areas by thresholding the cross-correlation values and a percentile method for selecting a threshold for each image. A histogram test eliminates false alarms. The intensity histogram of the detection and surrounding area is found and its number of peaks is examined. If the histogram contains two peaks, the area is considered suspicious; otherwise, it is eliminated from consideration.

Kegelmeyer detects stellate lesions using an analysis of the histogram of edge orientation of local windows and also Laws texture energy measures (23). Karssemeijer and Brake use statistical analysis of a map of pixel orientations to detect stellate patterns of spiculated masses (21). At each level of a multiscale approach, orientation is obtained

at each pixel by taking the maximum output of three-directional, second-order, Gaussian derivative operators. Two operators, sensitive to radial patterns of straight lines, are used as inputs to a classifier for the detection of stellate patterns.

Huo *et al* analyze patterns and quantify the degree of spiculation of the detection using radial edge-gradient analysis (19). Once an outline of a mass lesion is obtained, analysis of the neighborhood at the margin is performed to evaluate the margin spiculation.

Each of these systems uses different means for extracting the mass and various features for the classification of the masses. The databases used for algorithm development and testing are all different as is the size of images, number of gray levels, and difficulty of cases.

2.2.3 Database Comparisons. Appearing obvious from the brief descriptions above, many investigators are involved in the development of CAD methods for mammography. Although it would be attractive to be able to diagnostically compare these schemes, the results have been purposefully omitted. A qualitative comparison of various methods currently are not possible because of the use of different databases, with images varying in size, gray-level bit depth, and case difficulty, as well as having different means of evaluating results (13, 14, 35). It can not be assumed that a computerized scheme that achieves a high sensitivity with one database will achieve a similar performance level with another database or with an actual patient population (13, 35).

Chang *et al* attempt to display their system's robustness to change by testing it under different conditions. The system contains five stages where each perform an evaluation on the mammogram. Each stage is permitted to keep the one detection which scores highest on that stage's criterion. The five detections are fused to form the result. Chang attempts to show the robustness of the system based on its ability to perform while doing each of the following: 1) selecting a maximum of two suspicious mass regions at each stage, 2) eliminating any one individual stage, 3) adding noise, and 4) re-digitizing the mammogram and re-processing the image.

Nishikawa experiments with the effects of case selection on the performance of a single system (35). When testing the system on separate sets, he shows that the sensitivity can

range from 26% to 100% (at a specific false positive rate). By altering the test set by only 20% of its cases, the sensitivity can decrease by 15% to 25%. Since no practical means of comparing results exists today, using qualitative measures such as size, contrast, and level of subtlety of cases in a database, is suggested (35).

The ultimate test of any computerized analysis scheme is its ability to improve the performance of the radiologist (13, 14). Since CAD systems will be used as second opinions, the system may not have to be perfect. The overall accuracy of the system could possibly be less than that of the radiologist because the computer detections may not completely overlap those of the radiologist (13, 14). Best use requires radiologists to accept using a CAD system and learn how to best use it.

2.3 Summary

Mammograms may contain three indicators, calcifications, parechymal patterns, and masses, which provide information about the possibility of breast cancers. This thesis attacks the problem of mass detection for use as a second opinion to radiologists. Many groups have worked in this area. Their methods include bilateral-image subtraction, filtering, region growing, and template matching. Many different features, such as size, contrast, and textures, are extracted to try to reduce the number of false positives. At present, the performance of the systems can not be compared since databases and metrics differ. One means of comparison is by extensively characterizing the database used for each study (35).

III. Methods

3.1 Introduction

This chapter describes two major areas: 1) the database and 2) the several units forming the mass detection system.

3.2 Database

Mammograms used for this study were obtained through an agreement with the Wright-Patterson Air Force Base Hospital. The malignant cases were verified cases with malignant pathology between 1991 and 1995. The benign cases were chosen by selecting the benign cases closest in time to each malignant case (17).

Once selected, the mammograms were digitized using a Lumisys 200 automatic laser film digitizer. The full-breast films were digitized at a resolution of 100 μm with 12 bits of gray-scale per pixel. The digitizer ranges from 0 to 3.5 Optical Density (OD) at a resolution of 0.001 OD. Therefore, each pixel contains a value equal to 100 times its OD.

By cropping patient information and extraneous edges, database images were standardized to be 2048x1024 pixels to represent the 20.48cm x10.24cm of the original film. Pathology and location of the masses, as identified by a physician trained in radiology (17), were maintained for algorithm development and validation of results.

Table 1 Complete AFIT database statistics: area in number of pixels, diameter of circle with equivalent area, contrast, and difference in optical densities inside and outside of the mass.

		Area	Equivalent Diameter(mm)	Contrast	Difference in OD
Full Database	mean	11519	10.99	0.068	0.357
	standard deviation	12139	5.1	0.033	0.167
Malignant Masses	mean	12256	11.08	0.0680	0.366
	standard deviation	14794	5.8	0.0345	0.186
Benign Masses	mean	10724	10.90	0.0677	0.348
	standard deviation	8477	4.26	0.0315	.146

Since no valid means for comparison of results exists, researchers have indicated the best way to substantiate a breast cancer detection system is to detail the sizes and contrasts of the masses in the database (35). Histograms detailing the AFIT database are shown in Figure 1. The size and contrast information are obtained by first manually extracting the mass from the digitized mammograms, then calculating the statistics. The diameter is calculated by finding the diameter of the circle equivalent in area to the number of pixels forming the extracted mass. Size and contrast can be defined in a variety of methods.

One definition for contrast is in terms of differences in average OD as follows (52):

$$Contrast_{DiffinOD} = C_{in} - C_{out} \tag{1}$$

where C_{in} and C_{out} are the mean OD values of the area inside and outside the mass, respectively. The mean value outside the mass was calculated by finding the mean intensity of the area outside the mass border as shown in Figure 2.

Another definition for contrast is (33)

$$Contrast = \frac{C_{in} - C_{out}}{C_{in} + C_{out}} \tag{2}$$

where C_{in} and C_{out} are defined as previously stated.

The statistic for the database are found in Table 1. The statistics for each mass alone can be found in Appendix A. In order to classify the AFIT database as comparable to others

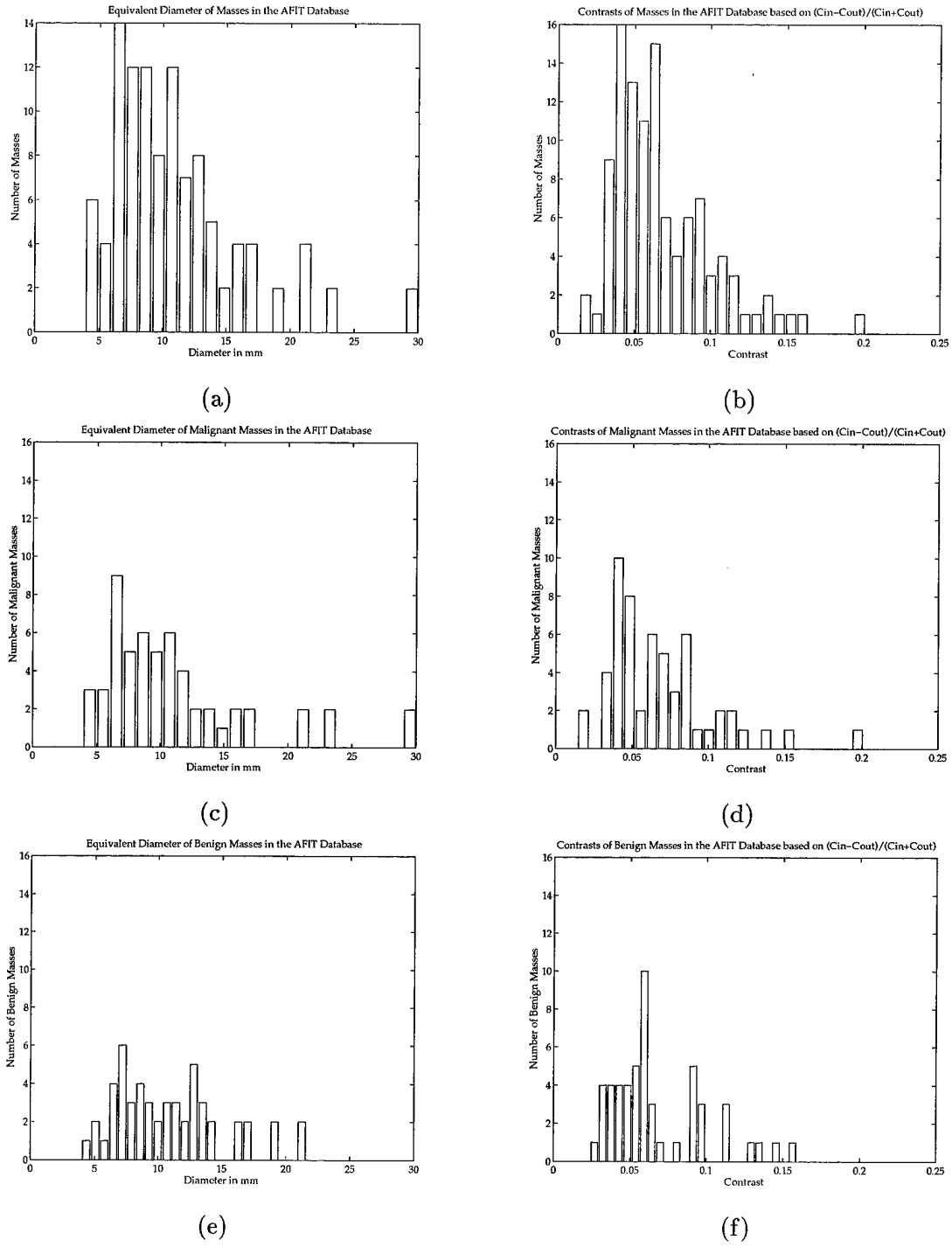

Figure 1 The first column contains the Histograms for Mass Sizes and the second column shows the Histograms for Contrast of the Masses. The rows are broken into (a and b) Complete Database, (c and d) Malignant Masses, and (e and f) Benign Masses. Note: all histograms are of the same scale. Contrast histograms using the difference in OD definition are not shown here, but may be seen in Figure 4.

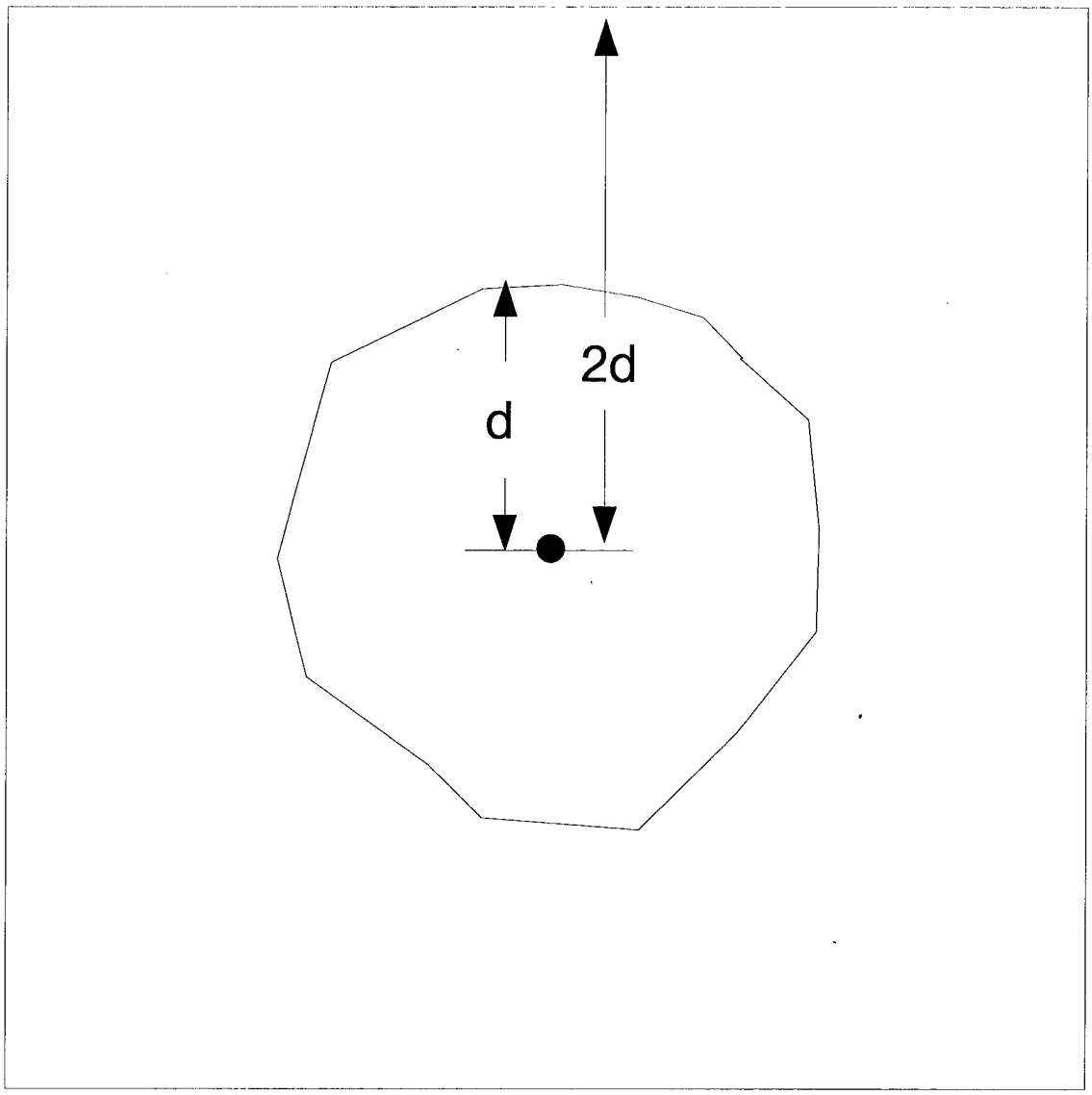

Figure 2 Box containing outside area is found by finding the distance, d, from the centroid to four points (immediately up, right, down, and left of the centroid) of the perimeter of the mass. The outside box is the box containing the points less than twice the distance from the centroid to selected perimeter point in each direction. This method allows contrast to be less dependent on the size of the mass, since the distance from the perimeter to the bounding box is not a fixed number.

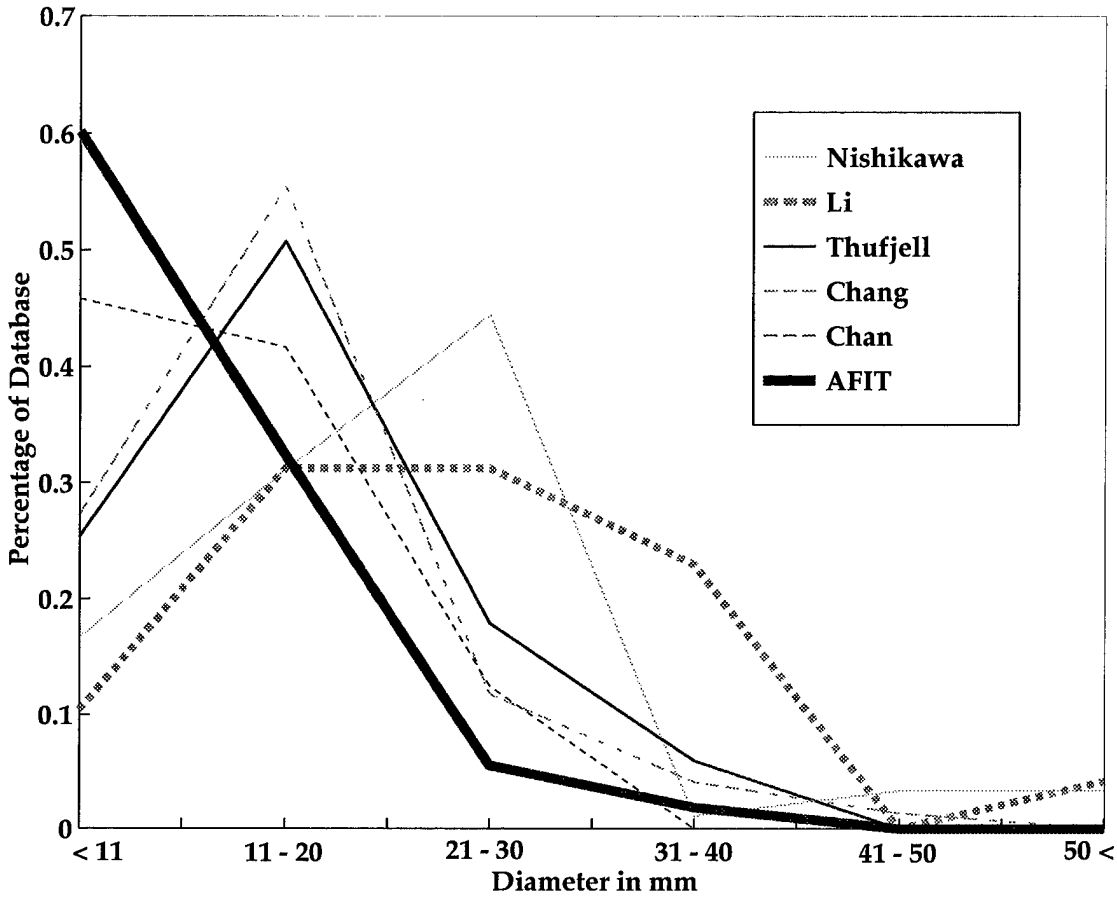

Figure 3 This figure compares the AFIT database to other databases. The AFIT database contains a much larger percentage of small masses than the other databases shown here.

Table 2 Size distribution comparison for several databases found in literature. This shows the percentages of masses less than or equal to a specified limit (11mm and 20mm.) This measure is important since smaller masses are typically more difficult to identify.

	% ≤ 11mm	% ≤ 20mm
Nishikawa	16.67	47.78
Li	10.42	41.67
Thurfjell	25.37	76.12
Chang	27.27	82.73
Chan	45.83	87.50
AFIT	60.19	92.59

in literature, a comparison of the sizes and contrasts of the masses is used. Figure 3 shows the size distributions of various databases found in literature (8, 9, 29, 35, 48). Table 2 compares the distributions in terms of percentage of the databases smaller than 11 mm and 20 mm. The AFIT database has the largest percentage of small masses, which are generally considered those more difficult to detect.

Another comparison of the AFIT database to others is by comparing the contrasts of the masses. Figure 4 shows the contrasts of the masses of the AFIT database and two others found in literature. Contrast for this comparison is the average difference in optical density of the mass and its surrounding tissue. No accepted definition has been established for the amount of surrounding tissue to use in the definition of contrast. Zheng compares several means for doing this and reported several statistics on his database (52). The numbers reported here are those he calculated using an outer area 25 pixels larger in four directions of the mass. Chang (9) uses a similar box that is 20 pixels larger than the largest axis of the mass. Both schemes are based on a resolution of 400 μm. As previously stated, contrast for the AFIT database is calculated using the outer box as shown in Figure 2. To translate this measure to terms similar to Zheng and Chen, consider that the average mass in the AFIT database has a diameter of 10.99 mm which at 400 μm is equivalent to 27.475 pixels. In Zheng's study, he shows that larger the outer boxes increase the measure of contrast (52). Therefore, the scheme used to calculate the contrast of the AFIT database is similar to the other two measures, but possibly slightly biased toward higher contrasts

Table 3 Complete description of number of images per case in the AFIT database. NOTE: Two 2-view cases, 1 malignant and 1 benign, contained two masses in each view.

# views/case	# Malignant Cases	# Benign Cases	Total
4	1	0	1
2	23	23	46
1	4	4	8
TOTALS	28	27	55

than the other databases. Even though its contrast is calculated with a larger window size, the AFIT database has the highest percentage of low contrast masses.

Since mass size and contrast has been shown to be indicative of the the difficulty of the database, these are the selected mean for evaluating the AFIT database and therefore results obtained using it. Both the size and contrast measures of the masses in the AFIT database show that it is a comparable if not a more challenging database than those described in literature. Overall, the masses in the AFIT database are small and have low contrast making this database challenging for breast cancer research.

The AFIT database contains a total of 55 cases containing 58 masses (104 images containing 108 masses). Most cases consist of two views, but 1 case had 4 views and 8 others had only a single view. Each view consists of one image. The number of images per malignant and benign cases is shown in Table 3.

Mammography cases typically consist of four films, two views of each breast. The details in Table 3 refer to the number of films for each cases in the database and not the actual number of films taken by the radiologist. The 4-view case in the database indicates that the patient had a mass in each breast creating a two 2-view case situation. A 2-view case contains the two images of the breast containing the mass. A 1-view case is a situation in which the radiologist could only locate the mass in a single view of that breast. The database contains two 2-view cases (1 malignant and 1 benign) containing two masses in each view.

The AFIT database consists of a balanced data set with approximately equal numbers of malignant and benign cases and masses. As many cases as possible were selected for this study to ensure a good cross-section of typical mass cases.

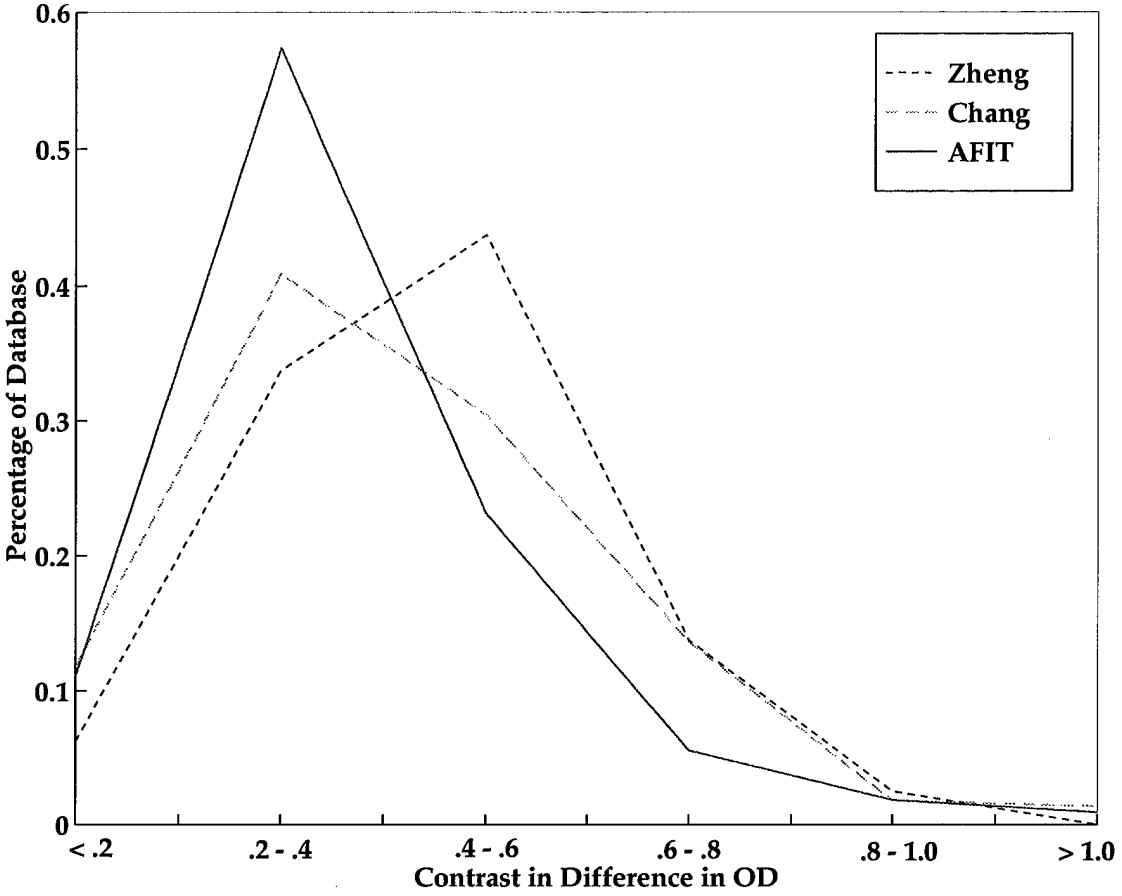

Figure 4 This figure compares the contrast of the masses in AFIT database to two other databases. The difference in OD is calculated using the mean OD inside and outside of the mass. The method used to calculate contrast for the AFIT database uses a larger outside area to compute the mean outer intensity. Therefore, the contrast is biased toward higher values than the other databases. However, the AFIT database contains the largest percentage of low contrast masses.

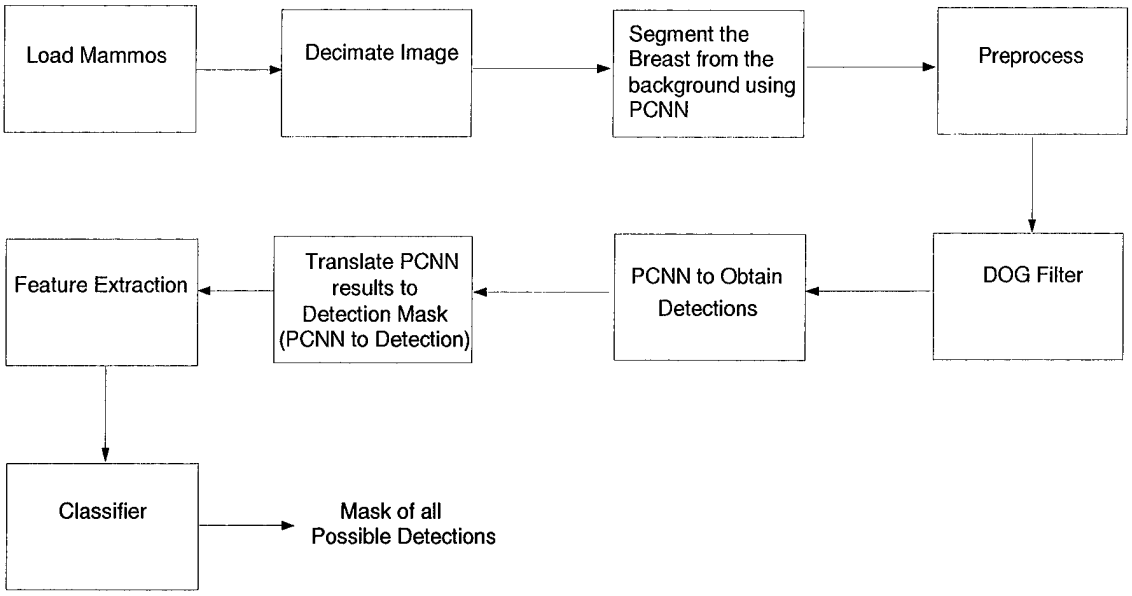

Figure 5 Mass Detection System using a Difference of Gaussians filter and Pulse Coupled Neural Network. The systems takes a 2048x1024 mammogram as input and outputs a mask of all possible detections.

3.3 Mass Detection System

The system developed for this thesis is composed of six major components as shown in Figure 5. The system has been designed to take as input a 2048x1024 pixel digitized mammograms with 12 bits of gray-scale information per pixel. The output of the system is a mask of all suspicious areas. The six components of the system are described in the following subsections.

3.3.1 Segmentation of Tissue from Background. Properly segmenting the breast tissue from the background of the digitized mammogram is important to two parts of the mass detection system. First, the preprocessor uses the breast mask to manipulate the decimated image for better processing. The mask allows the preprocessor to enhance just the breast tissue or to vary the background. Second, the breast mask is used to ensure that all detections are within the tissue. Segmentation of the breast tissue from the background is done using a pulse coupled neural network (PCNN). To understand how segmentation is performed, the PCNN needs to be explained.

3.3.1.1 Pulse Coupled Neural Network. The PCNN is a physiologically motivated artificial neural network. The basic details of how the PCNN works and the parameters used for this research will be explained. More information on the biological and theoretical foundations for the PCNN can be found elsewhere (5, 6, 11).

The PCNN for this research was designed to take as input a two-dimensional image. Similar PCNNs have been previously used by AFIT students for MRI segmentation and image fusion for object detection (1, 5), however mass detection using the PCNN has never been previously investigated.

The significance of the PCNN is its modulatory behavior of neurons. Each pixel of an image is considered a neuron. Each of these neurons are characterized by a modulatory inter-neuron linking similar to the interaction of cells in primate primary visual cortex.

A neuron will respond or "fire" when its internal activity reaches a certain threshold. The stimuli driving this internal activity is the neuron's feeding input and linking connections. An example of feeding and linking connections of a single neuron within the PCNN is shown in Figure 6.

The equation defining the internal activity for this PCNN is

$$U_k = F_k(1 + \beta L_k) \tag{3}$$

where F_k is the feeding input to the k^{th} neuron, L_k is the linking input to the neuron, and β is the linking strength of the connections between neurons. When the internal activity of the k^{th} neuron, U_k, exceeds a threshold, θ_k, the neuron will fire. For this application, F_k is the pixel intensity of the k^{th} pixel of the input image and the L_k is the sum of the inputs to the k^{th} neuron from its connections to its neighboring neurons based on its linking radius. In other applications, F_k can be effected by its neighboring pixels based on its feeding radius. For this application, the feeding radius has been set to zero. Similar to neighborhood averaging, linking radius size will determine how many of a neuron's neighbors will be effected when it pulses (5).

Theoretically, the operation of the PCNN is temporally based. All neurons are considered to have fired at $t = 0$. Normalization by the maximum intensity brings all

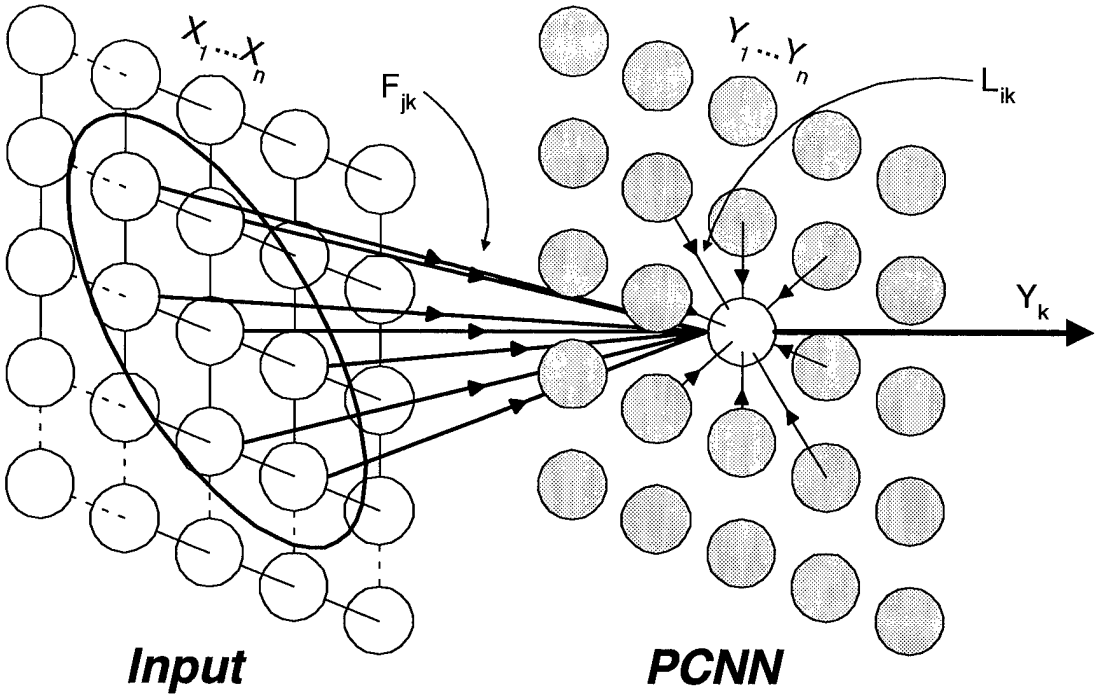

Figure 6 The connectivity of a single neuron (Y_k) with a linking radius of 1 is shown; Thus, Y_k receives its feeding input through F_k and its linking input through L_k where j are the nodes providing the feeding input and i are the 8 neighbors providing the linking input. Notice that this F_k is the result with feeding radius of 1. Illustration provided by Capt. Randy Broussard (AFIT/DS/ENG/97-02).

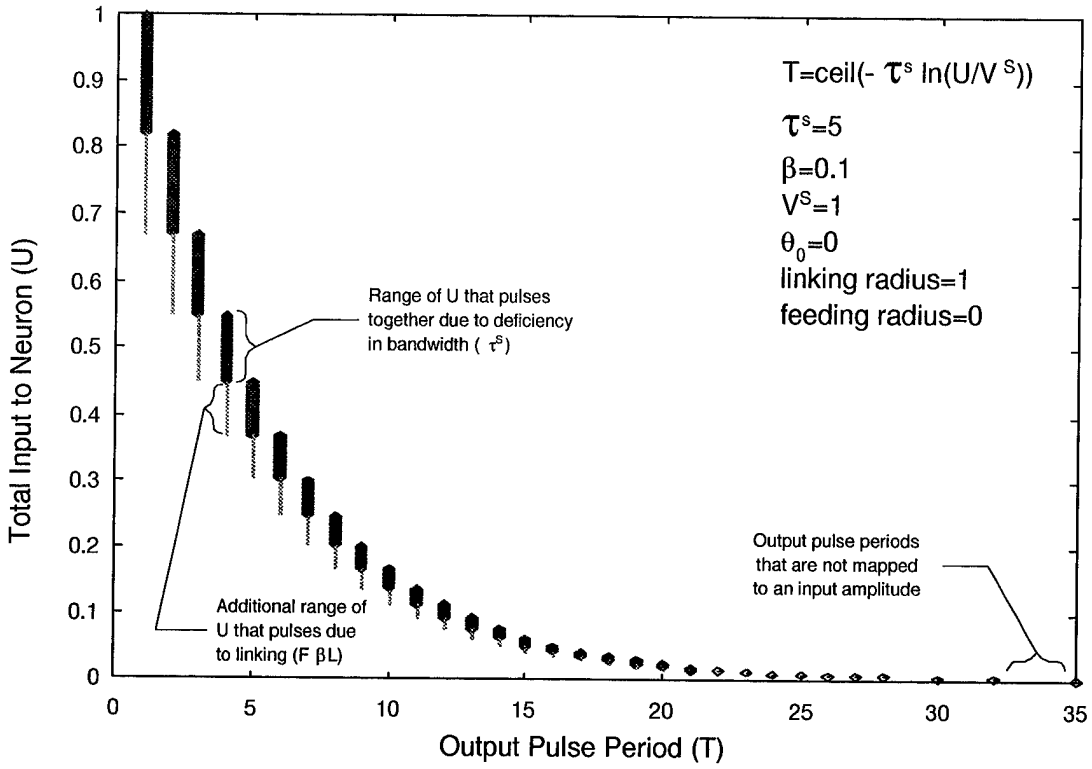

Figure 7 As timesteps increase, the θ_k or amount of Total Input to a Neuron decreases exponentially making it possible for more neurons to fire. Recall that all neurons fired at $t = 0$ and that the intensities have been normalized so the maximum value of U_k at $t = 1$, timestep 1, is 1.0. Illustration provided by Capt. Randy Broussard (AFIT/DS/ENG/97-02).

inputs between 0 and 1. At $t = 1$, the neurons with a normalized magnitude of 1 will fire. Once a neuron pulses, its linking neighbors receive a contribution through their linking connection. Although a neuron may not have a high enough feeding input, F_k, it may receive sufficient linking, L_k, to fire. This will occur when $F_k = (1 + \beta L_k) > \theta_k$. Once this neuron fires, all its neighbors will receive a pulse. A steady state occurs when no more neurons will fire at $t = 1$. The timestep is then increased to $t = 2$, θ decays, and the process repeats itself until either all neurons have fired or the last timestep to be used, τ_s, is achieved.

As time increases, θ_k, the level of U_k, necessary to fire, decays exponentially. As seen in Figure 7, the relationship of number of timesteps utilized to the time constant value is

significant. When using the first 10 timesteps, the advantage of the PCNN to thresholding is shown by the "tail" or additional range of U_k that pulses due to linking. For later timesteps, this tail nearly disappears making the PCNN output at these timesteps quite similar to simple thresholding of a section of the dynamic range.

The PCNN can be used in a variety of ways, two of which will be explained. First, the PCNN output can be divided into two classes, pixels which have pulsed and that have not. Second, classes can be assigned based on the timesteps when pixels pulsed. Thus, a pixel pulsing at $t = 5$ would be a member of class 5.

This mass detection system utilizes both of these methods. Using the first method, the PCNN segments the breast tissue from background creating a breast mask. Later in the system as discussed in Section 3.3.5, the PCNN identifies mass-like objects from the DOG filter output using the second method. Other uses for the PCNN for mass detection have been investigated and show promise. These techniques will be further explained in Section 5.2.

After experimentation with the PCNN for full-breast segmentation, the following parameters are selected: $\beta = 1$, $LR = 1$, $T = 3$, and $\tau_s = 5$. These parameters were chosen so that the whole breast would pulse and background would not. The sensitivity of these parameters are shown by Figure 8. With the parameters set as in Figure 8a, nearly all of the images in the database would segment properly. However, in an image, such as a002b00m shown in Figure 8b, a portion of the breast appears to be close to background gray-scale. By using more timesteps and dividing the results into two classes based on whether pixels pulsed or not, images like a002b00m, can be segmented properly without effecting the results for the other images. The success of this technique is shown in Figure 8d.

3.3.2 Decimation. Since the mammograms are digitized at 100 μm and the focus of this research is masses ranging from less than 0.5 to greater than 2 cm (5000 to 20000 μm) in diameter, the images can be decimated to drastically reduce the computational intensity of the system. Decimation is typical for mass detection (23, 37). Through experimentation, decimation by a factor of 4 in each direction was selected. The effects of this decimation on

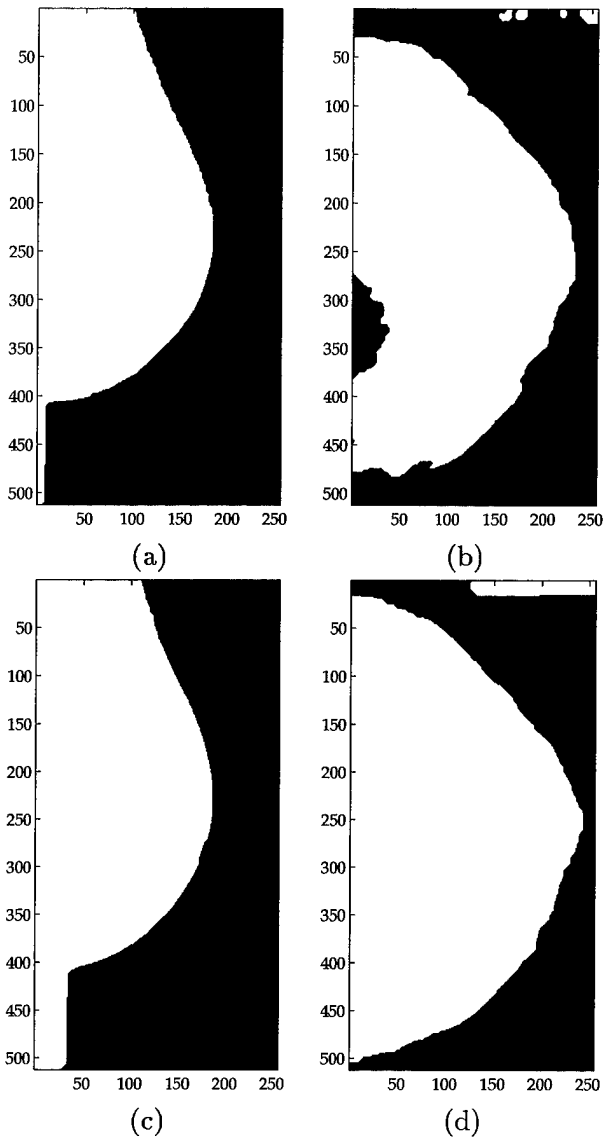

Figure 8 These are two sets of results of using the PCNN to segment the breast tissue from the background in two mammograms. (a) and (b) are images a001d00m and a002b00m processed using the same PCNN parameter. The settings used for (a) and (b) properly segment most images, however difficulties arise for images such as (b), which contain portions of the breast, that did not block the x-rays. Therefore, the image in those areas appears similar to background intensity. (c) and (d) were processed with different parameter settings. The combination of these settings and the use of multiple timesteps to assign class labels allow the breast tissue to segment properly in images such as a002b00m.

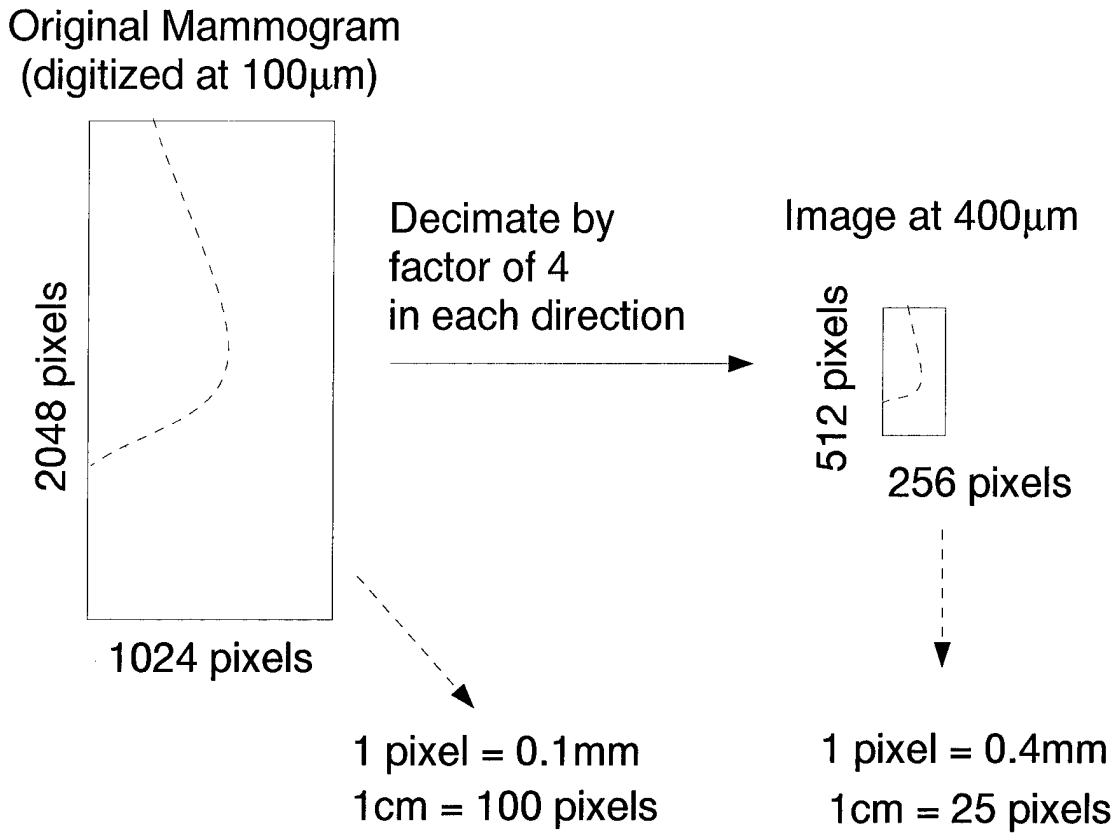

Figure 9 When decimating by a factor of 4 in each direction, the amount of information will be 1/16th the original as visually shown. The diameter in pixels representing a 1cm mass is only decreased by 1/4, since diameter is 1-dimensional.

the image size is shown in Figure 9. The effect decimation has on identifying a 1 cm mass is that the task of locating an object with a 100 pixel diameter is changed to detecting objects with a diameter of 25 pixels. The effects of this in the whole range of images is that masses ranging from 0.5 to 2 cm in diameter will be 12.5 to 50 pixels in diameter respectively.

The lower resolution did not lose important information for finding masses from the mammograms. Preprocessing the 2048x1024 image with an averaging filter prior to decimation was not necessary due to the size of the objects being detected.

3.3.3 Preprocessing. Once decimated, the image needs to be improved to enhance the probability of later detection, as well as to reduce the probability of later false detections. Preprocessing for a CAD system is different than preprocessing for a human vi-

sual and recognition systems. One form of preprocessing generally used to enhance images for the human visual system is histogram equalization. Basically, histogram equalization spreads the gray levels of the image increasing the dynamic range of gray levels and, consequently, producing increased contrast. For further discussion and derivation see (15). The result of histogram equalization on one mammogram is shown in Figure 10b.

An alternate means of preprocessing is to find the mean of the intensities within the breast tissue and make the entire background this level. This technique reduces the extreme difference between the breast tissue and background. By doing this, the DOG filter does not detect the edge of the breast as strongly and therefore allows for better detection of objects within the breast. Yet another technique is to mirrorpad the image about the breast edge. This method also attempts to reduce processing edge effects due to the intensity differences of tissue and background by reflecting the breast tissue about the breast edge from the segmentation mask. Examples of these techniques are shown in Figure 10(c,d). Comparison of results obtained using these methods are presented later in Chapter IV.

3.3.4 Difference of Gaussians (DOG) Filtering. As discussed previously in Section 2.2.2, DOG filtering is widely used in breast cancer detection systems. This section will briefly discuss how a DOG filter is created, how it works, and how it may be tuned for this database.

3.3.4.1 Definition and Background. The difference of two Gaussian probability density function distributions (DOG) filter is motivated by the first stages of visual processing (30). The visual system contains orientation and spatial frequency selective channels. Each point in the visual field has four size-tuned filters. The spatial receptive fields of each of these filters has approximately the shape of a DOG.

The two-dimensional DOG filter is defined as

$$G(x,y) = c_1 exp(-\frac{x^2+y^2}{2\pi\sigma_1^2}) - c_2 exp(-\frac{x^2+y^2}{2\pi\sigma_2^2}) \quad (4)$$

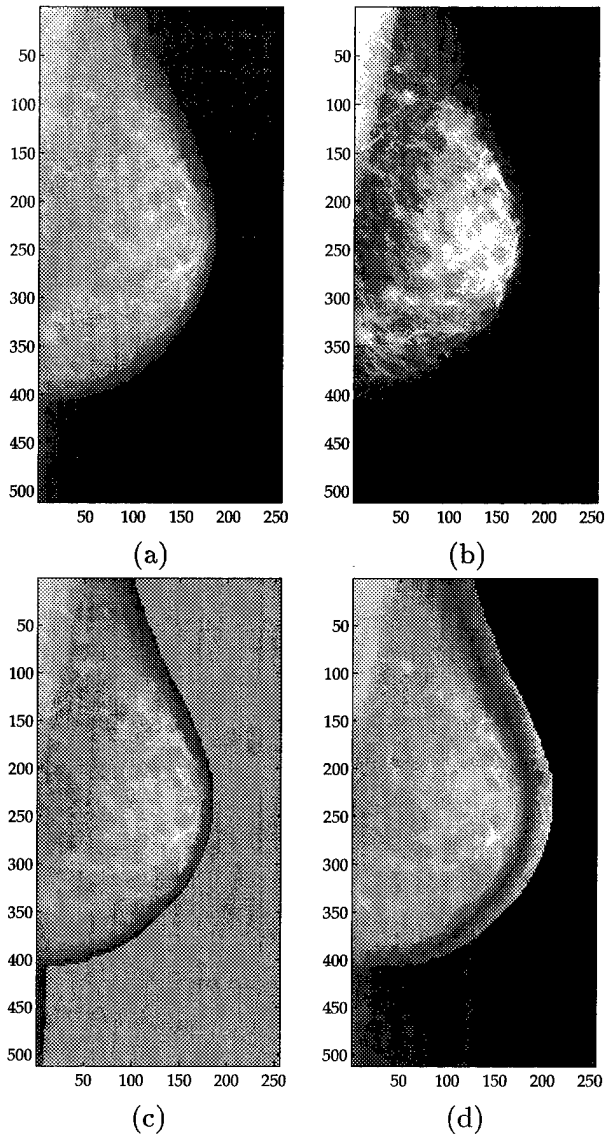

Figure 10 Three techniques for preprocessing a breast image before DOG filtering. (a) Original decimated mammogram, (b) Histogram equalized, (c) Technique making the background equal to the mean intensity of breast tissue, and (d) Mirrorpadding about the breast edge.

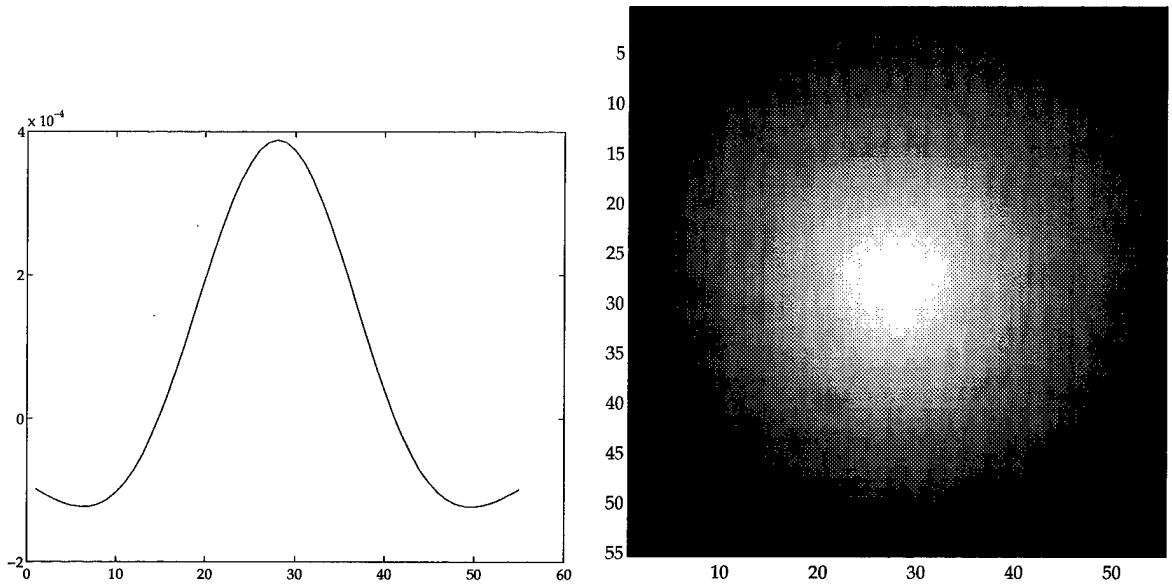

(a) (b)

Figure 11 The (a) 1-dimensional and (b) 2-dimensional Difference of two Gaussian distributions (DOG) kernels used to filter the images. This particular kernel has a dogsize or diameter at zero crossing of 25 pixels (equivalent to 1 cm). The gray-scales in (b) have been scaled from the largest negative (darkest) to greatest positive (brightest).

where c_1 and c_2 normalize the area under each Gaussian to unity, σ_1 and σ_2 represent the standard deviations, and x and y are the horizontal and vertical indices. The best approximation from an engineering perspective is when the Gaussians have standard deviations in the ratio 1:1.6 (30). For this reason, this ratio was maintained for this thesis. One and two-dimensional views of the DOG in the spatial domain are shown in Figure 11.

3.3.4.2 Functionality. The DOG can be tuned spatially or in the frequency domain. The functionality of this will be shown through example. Figures 12 and 13 show the results of DOG filtering two mammograms.

The two different sizes of masses show the difficulty of detecting masses with a single DOG filter. As shown in Figures 13c and 13d, when the DOG filters a digitized mammogram, densities of the size of the DOG are enhanced whereas areas which are much smaller or larger are eliminated. If the DOG filter is tuned for smaller masses like the one in a001d00m, larger masses, such as the a002b00m mass, are missed. The converse

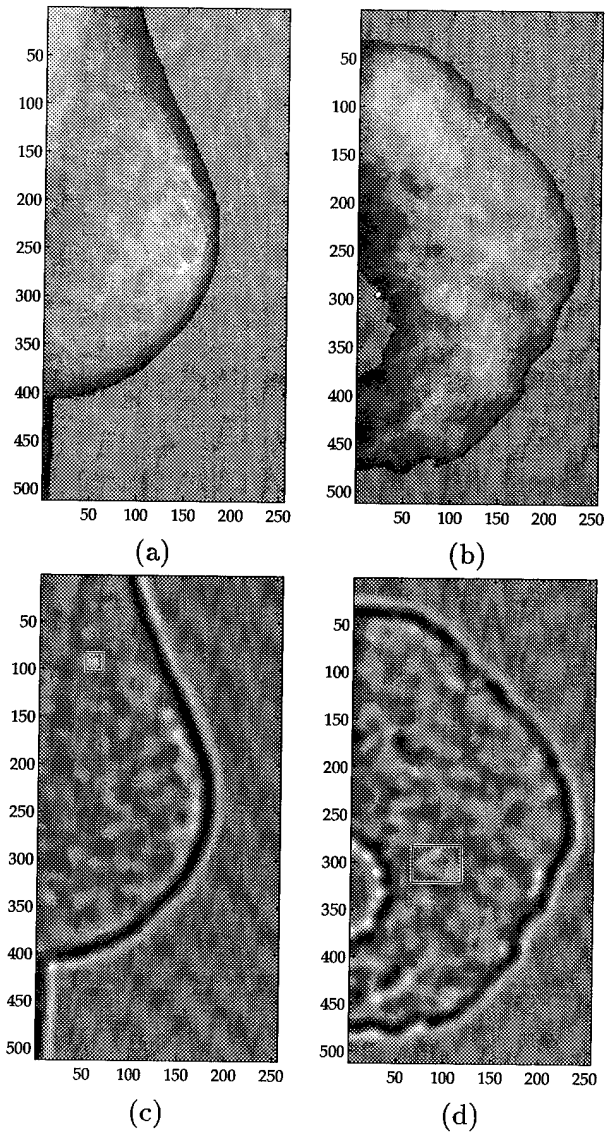

Figure 12 Original decimated mammograms, a001d00m and a002b00m, are shown in (a) and (b) respectively. (c) and (d) are the results of filter with a DOG filter with dogsize of 10. By doing this, small objects like the mass in a001d00m are enhanced, while only, at most, a small portion of the mass of the size of a002b00m will be found. The truth box is provided to show the goal of filtering.

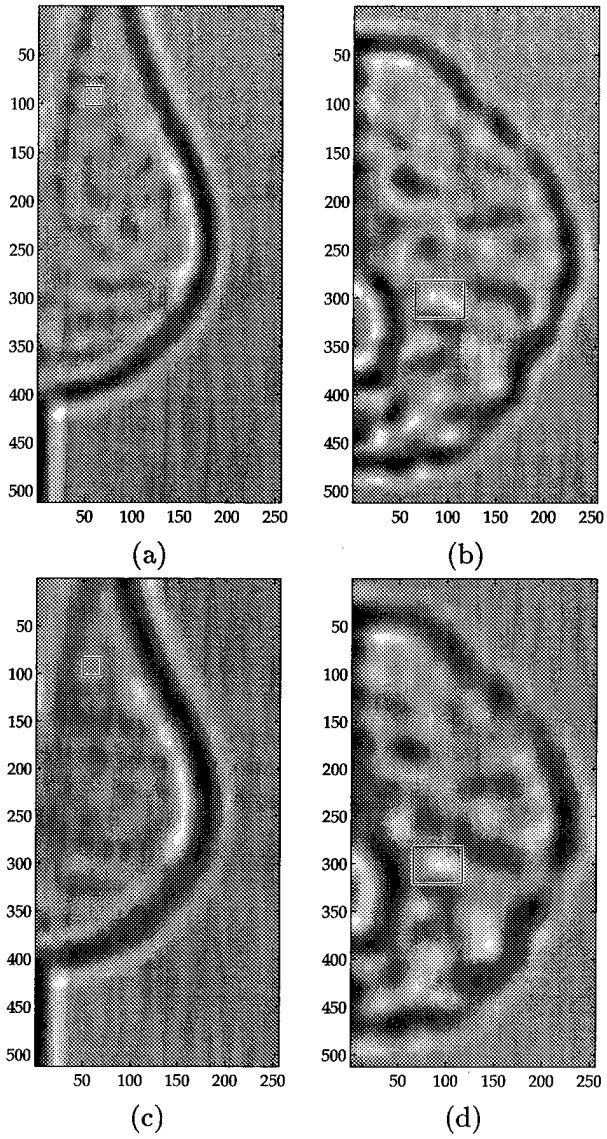

Figure 13 (a) and (b) are the result of DOG filtering with a dogsize of 20. (c) and (d) were created by filtering with a dogsize of 30. Through the course of these two figures, the size restriction of a DOG filter can be seen. The mass in a001d00m was best found using a smaller DOG kernel. The mass in a002b00m needed a larger DOG kernel to be properly identified.

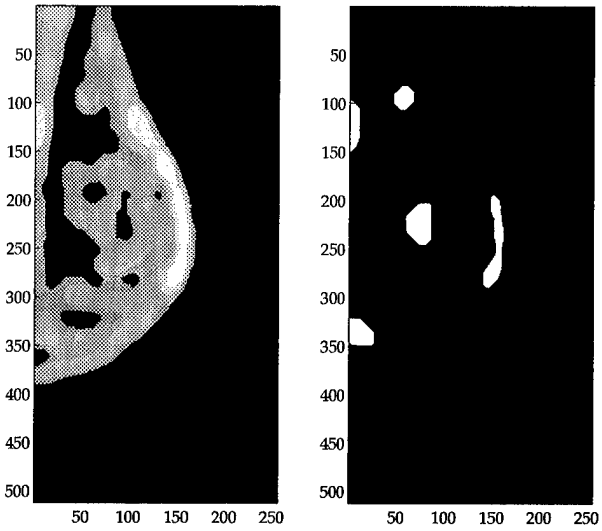

Figure 14 The results of the PCNN on a DOG filter image is shown in (a). This was accomplished with $\beta = .35$, linking radius $= 1$, $T = 50$ timesteps, and $\tau_s = 100$. (b) shows how the PCNN output can be turned into a detection mask.

of this is also true. Therefore, the DOG filter needs to be designed to find as wide a range as possible. An intelligent postprocessor to the DOG filter also aids in detecting masses even after being filtered with other than an ideal sized filter.

3.3.5 PCNN to Obtain Detections. Another use of the PCNN, described in Section 3.3.1.1, is as an object detector. The DOG filtered image is used as the input to this second PCNN module. The desired output is an image with the information necessary to extract mass-like objects from its surroundings. The results of using the PCNN for object detection are shown in Figure 14.

The PCNN parameters are adjusted through experimentation to reach a range where the PCNN could detect masses from the DOG filter output. These PCNN parameter adjustments are needed for use as an object detector instead of a full-breast segmentor. For object detection, localized linking is desired instead of linking within the whole breast, but linking strength, β still needed to be strong enough to make detections large enough to be considered masses. A detection of a small number of pixels would be disregarded since masses are relatively larger areas. For this reason, through experimentation β was

found to work best in the range from 0.3 to 0.4 while the linking radius, LR, remains 1 so that each pixel still connects only to its 8 neighbors. Since masses will not always be the most intense areas in the DOG image, a means of detecting these areas is needed. By increasing the theta time constant, τ_s, to 100 and by using 50 timesteps of these 100, the PCNN was allowed to work in the zone where linking works best. By using 50 timesteps, masses with low global intensity, but with a local peak, are still detectable. A method is now needed for translating the results of the PCNN into a detection mask.

3.3.6 PCNN to Detection Mask. The PCNN to Detection Mask module takes the PCNN image as input, searches each timestep, also called "layers", for areas of the correct size that pulse prior to its surroundings, and creates as output a mask of all possible detections. The process of evaluating each possible detection of each layer of the PCNN image is best described by the following steps with their accompanying images as well as a flow diagram seen in Figure 15.

Recall that pixels of the input image will contain the value of the timestep when each pulsed; For example, a pixel which pulsed at timestep 10 will have a value of 10 and a pixel that did not pulse within the number of timesteps will contain a zero.

1. Make an image of the first timestep ($t = 1$). (Figure 16b)
2. Separate image into individual detections of this PCNN slice, since multiple areas can pulse at a single timestep. (Figures 16c)
3. Examine one detection or blob. (Figures 16d)
4. Calculate the area of the blob.
5. If $122 < area < 1963$ (or $0.5cm < diameter < 2cm$), continue, else go to 3 and look at the next blob.
6. For $t = 1$ add all blobs directly to the detection mask and go to step 1 and examine the next timestep slice.
7. Check to see if the blob is a doughnut. (Figure 17)

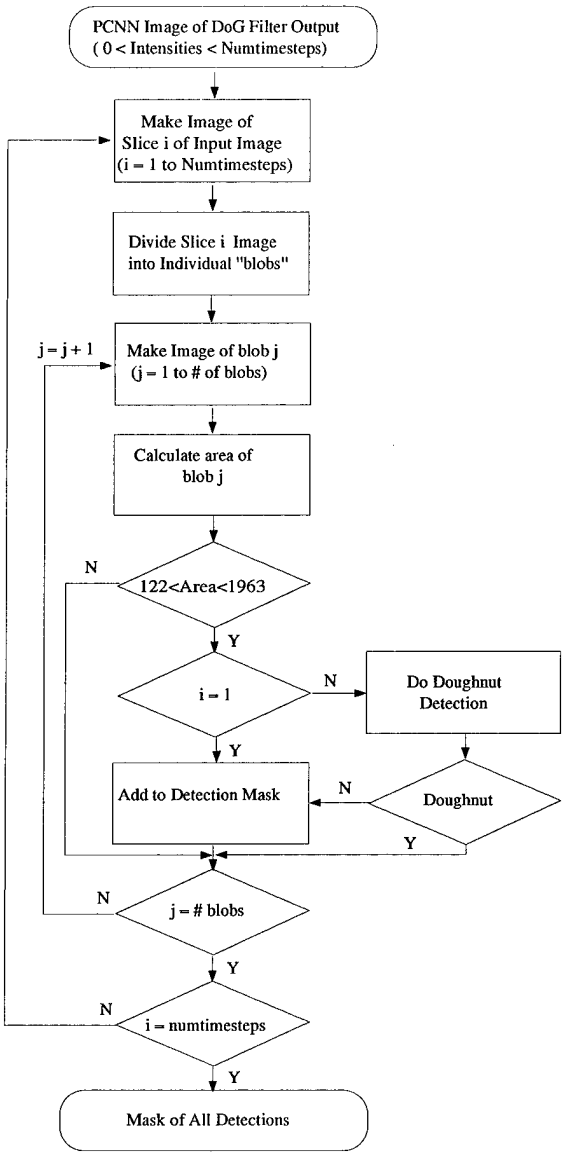

Figure 15 The PCNN to Detection Mask module creates an output of all possible detections. The module receives as input an image created by using the PCNN on the output of the DOG filter. A detection mask is created by iteratively examining each "blob" of each timestep slice. A "blob" is a termed used to refer to possible detections in a timestep.

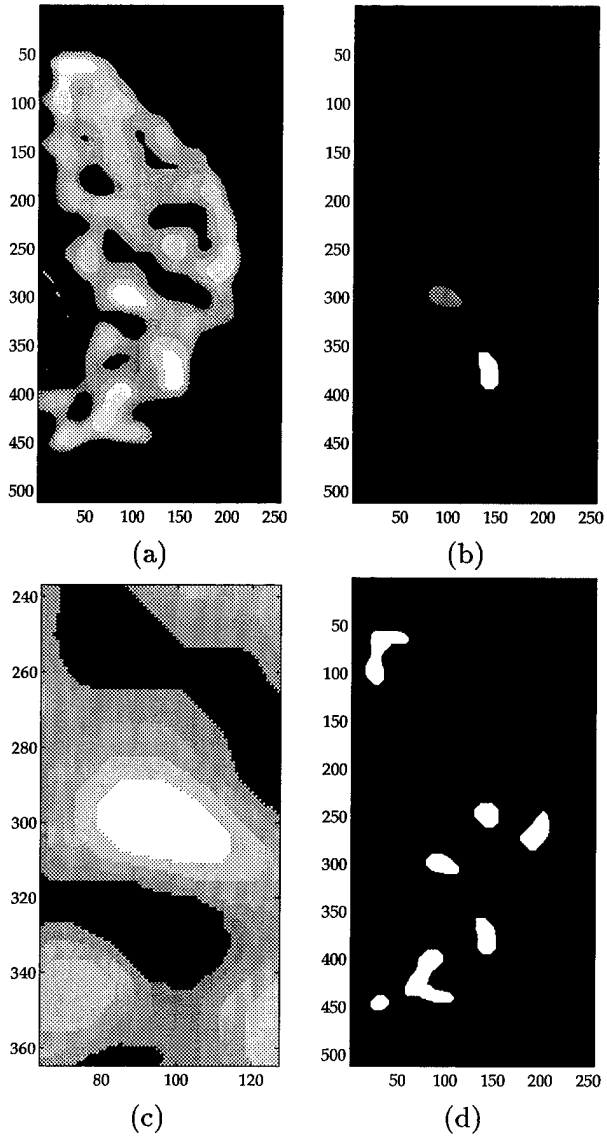

Figure 16 The PCNN output for the DOG image of a002b00m is shown in (a). (b) contains everything that pulsed at the first timestep, $t = 1$ and shows how each blob is labeled (given a unique value) for individual inspection. (c) shows one such blob which will be used to demonstrate doughnut removal. The first doughnut situation occurs at $t = 14$. (d) contains all blobs which made it through the detection scheme through the first 14 timesteps.

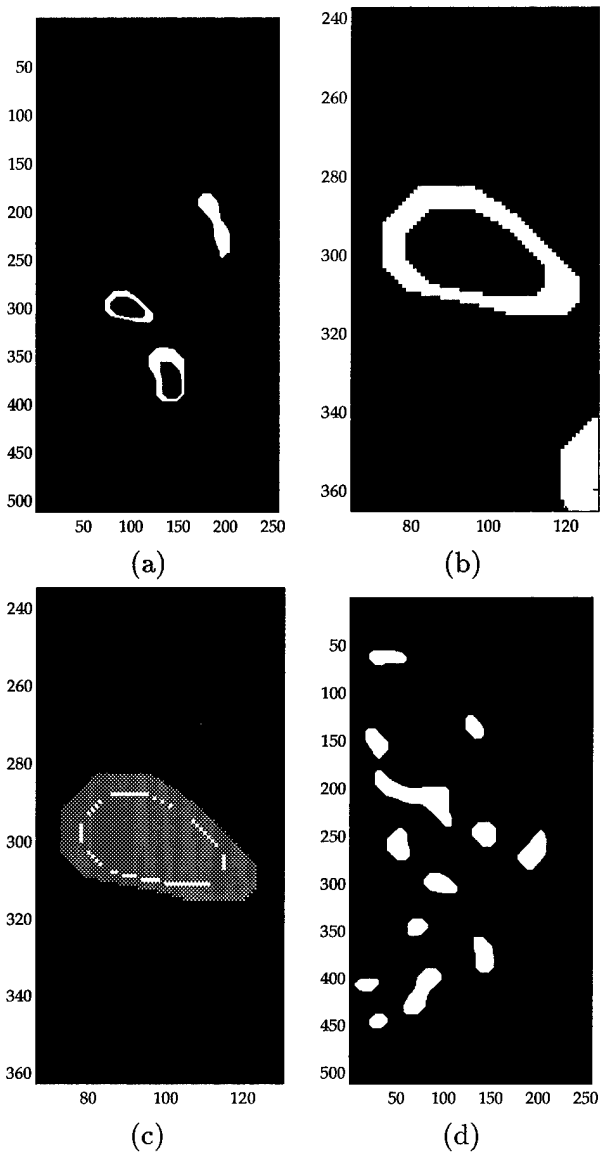

Figure 17 The pixels that pulse at $t = 14$ are shown in (a). There are two doughnuts at this timestep. The doughnut in (b) will be analyzed. (c) shows overlaying the doughnut in (b) and the dilated image of all prior pulsed pixels. Since an overlap existed, the doughnut was eliminated and not included into the detection mask shown in (d). This mask shows the complete results of this mammogram at the output of the PCNN to Detection stage.

(a) Take all previous timesteps and create an image of all pixels which pulsed at those timesteps.

(b) Dilate this image once.

(c) Check for an intersection of the blob image and the dilated image.

(d) If an intersection exists, eliminate blob from consideration, else add blob to the detection mask.

8. Perform steps 3 through 7 until each blob at this timestep has been examined.
9. Perform steps 1 through 8 incrementing the timestep each time until all valid timesteps have been analyzed.
10. Detection mask is sent as output of module. (Figure 17d)

Some comments about this process need to be presented. Since the PCNN normalizes intensities prior to pulsing, it is guaranteed that something will pulse at the first timestep, $(t = 1)$. Also, the blobs at the first timestep do not need to go through the doughnut stage, since they are first to pulse and could not be a doughnut. In step 4, area is calculated as the number of pixels forming the blob under consideration. The purpose of the area check in step 5 is to keep only those blobs whose equivalent circular diameter would be between 0.5 and 2.0cm. The valid timesteps, referred to in step 8, are those which have pixels that have pulsed since each timestep is not guaranteed to have had pixels pulse. The output of the PCNN to Detection module is a binary mask of all areas of local maxima with areas in the range of 122 to 1963 pixels.

3.3.7 False Positive (FP) Reduction. Once the detection phase of a pattern recognition system has selected all possible detections, feature extraction and classification need to be performed to reduce the number of false detections. This is done by calculating features from all possible detections and using a classifier to reduce the number of false detections while keeping the true positives (TPs). The following subsections will address the features and the classifier used for FP reduction.

3.3.7.1 Feature Extraction. A total of 34 features are extracted from each detection. These features are divided into two categories: morphological and textural.

The purpose of using morphological features is to keep detections that have mass-like shapes, locations, and areas. Circularity measures make good features because the density patterns of actual masses are generally more circular than those of glandual tissues or ducts (50). These circularity features, as well as other morphologically based features, make up 9 of the 34 features. The nine features are circularity, rectangularity, compactness, four normalized radial length features, minimum distance to border, and the area of the object.

Circularity, rectangularity, and compactness, the first three features, provide a measure of the overall shape of the tumor without specific detail to the tumor boundary. The circularity feature is found by creating a circle with an area equivalent to the object area, centering this circle at the object's centroid location, and analyzing the overlap (37). Circularity is defined as

$$Circularity \equiv \frac{area(A_{obj} \cap A_{eq})}{area(A_{obj})}, \tag{5}$$

where A_{obj} is the area of the object and A_{eq} is the area of the equivalent circle. Figure 18 shows an example of circularity and rectangularity. Rectangularity is defined as (37)

$$Rectangularity \equiv \frac{A_{obj}}{A_{bb}}, \tag{6}$$

where A_{bb} is the area of the minimum sized bounding box completely containing the object.

Compactness is defined as (24, 38, 43)

$$Compactness \equiv \frac{P_{obj}^2}{A_{obj}}, \tag{7}$$

where P_{obj} is the number of perimeter pixels of the object. Compactness is a measure of how the perimeter pixels vary in relation to the center. A circle would have a lower compactness than a jag- edged object.

The four normalized radial length features provide more details about the tumor boundary than the gross shape features, such as circularity (24). The radial length is defined as the Euclidean distance from the tumor centroid to each of the points of the

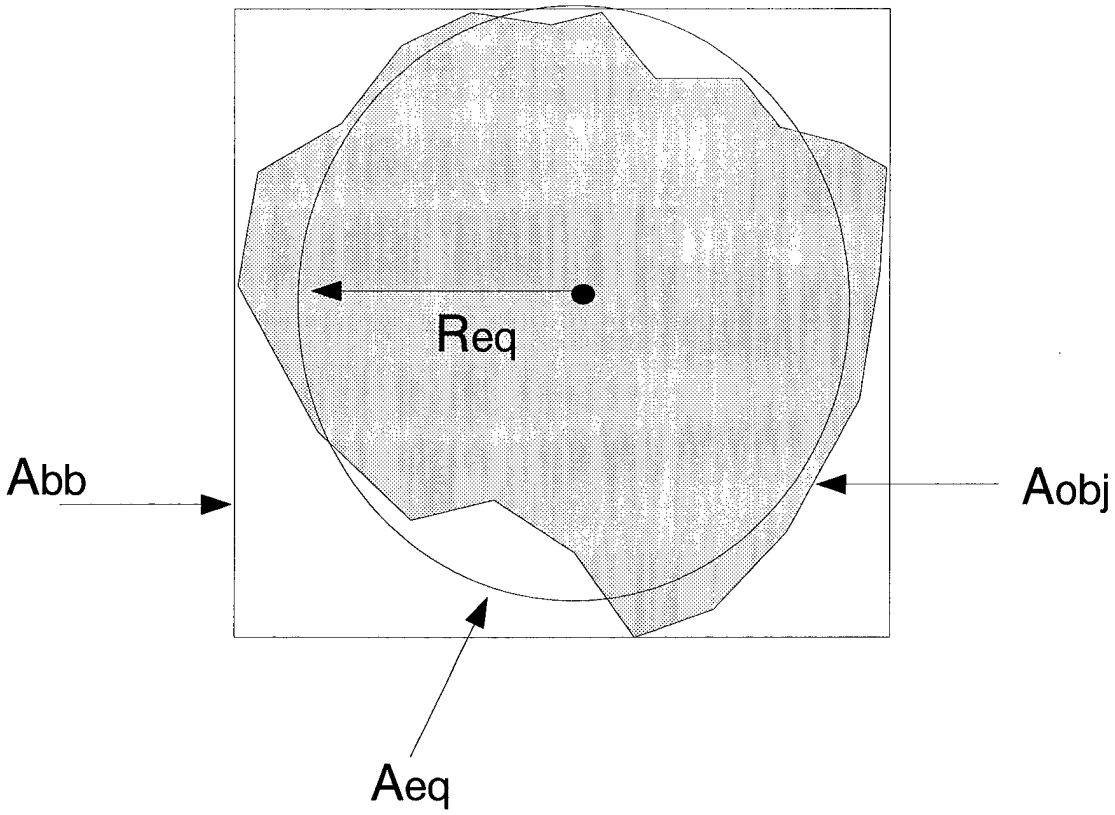

Figure 18 Circularity and rectangularity defined pictorially as defined in equations (4) and (5). The circle is the circle with the equivalent area of the detection. The rectangle is the bounding box which completely contains the detection.

tumor perimeter and normalized by dividing by the maximum radial length (24). The normalized radial length (NRL) features of mean, standard deviation, area ratio, and zero crossing count are calculated based on the following definitions. The NRL plot is the border of the detection stretched into a one-dimensional plot based on the NRL.

The mean and standard deviation of the NRL line plot for tumor i are calculated as

$$\mu_i \equiv \frac{1}{N}\sum_{k=1}^{N} r_k \tag{8}$$

$$\sigma_i \equiv \sqrt{\frac{1}{N}\sum_{k=1}^{N}(r_k - \mu_i)^2} \tag{9}$$

where r_k is the value of the normalized radial length at pixel k along the tumor perimeter (x_k, y_k), μ_i is the mean of the normalized line plot, σ_i is the standard deviation of the normalized line plot, and N is the number of pixels in the tumor perimeter.

The area ratio finds the intersection of the circle with a radius equal to the mean NRL and the tumor when the circle is positioned at the centroid of the tumor. The area ratio is defined as

$$AreaRatio \equiv \frac{1}{N\mu_i}\sum_{k=1}^{N}(r_k - \mu_i) \tag{10}$$

where

$$\text{Area Ratio} = 0 \ \forall r_k < \mu_i. \tag{11}$$

The zero crossing count feature gives detailed information about the tumor boundary. The zero crossing count is simply the number of times the line plot of the tumor boundary crosses the mean radial length or

$$ZCC \equiv \text{number of zero crossings of } \{r_k - \mu_i\}_{k=1}^{N}. \tag{12}$$

Table 4 Laws five 1-dimensional kernels or 5-vectors. The kernel names and corresponding labels are line (l), spot (s), ripple (r), edge (e), and wave (w).

label	kernel
l	[1 4 6 4 1]
s	[-1 0 2 0 -1]
r	[1 -4 6 -4 1]
e	[-1 -2 0 2 1]
w	[-1 2 0 -2 1]

Table 5 This l5l5 kernel is an example of a Laws 5x5 convolutional kernel.

1	4	6	4	1
4	16	24	16	4
6	24	36	24	6
4	16	24	16	4
1	4	6	4	1

The last two features in this category are area and minimum distance to the border. The area is calculated by summing the number of pixels forming the mass. The minimum distance to the border feature uses information about the location of the tumor to aid in reducing false alarms. Generally, most detections along the breast edge are false alarms due to the filtering of the image. Tumors are typically found in the interior of the breast further away from the skin (3).

Since the morphological features are not able to completely differentiate between the masses and the false detections, features utilizing information from the pixels interior to the detection are desired. A set of such features are found using Laws texture energy measures (28). These features have previously been used for breast cancer detection (22, 23, 39). Laws created five one-dimensional kernels, which may vary in length; they were chosen to have a length of five for this research and are shown in Table 4.

A 5x5 kernels is generated by convolving a vertical 5-vector, such as l5, with a horizontal 5-vector(28). This operation may also be considered as a cross-product or vector multiplication. Each 1-dimensional kernel is multiplied by the transpose of itself and each of the four others to create twenty-five 5x5 kernels. The example shown in Figure 5, the l5l5 kernel, is the result of the l5 kernel vector multiplied by its transpose. These kernels

Table 6 The maximum result of each Laws 5x5 convolutional kernel when convolved with an image with a maximum gray-scale value of 4095.

r5r5	524160	e5s5	49140
l5s5	131040	l5e5	196560
w5r5	196560	s5s5	32760
s5e5	49140	e5w5	73710
l5r5	524160	l5w5	196560
s5l5	131040	s5r5	131040
s5w5	49140	r5s5	131040
r5l5	524160	r5e5	196560
r5w5	196560	e5l5	196560
e5r5	196560	e5e5	73710
w5l5	196560	w5w5	73710
w5e5	73710	w5s5	49140
l5l5	1048320		

are then used to calculate the texture of the detections. The feature is extracted of each of the 25 kernels using the following steps:

1. Extract from the original decimated image, a box containing the detection with a border the size of the kernel about the extreme points of the detection.
2. Convolve the kernel with the box.
3. Sum the absolute value of the parts of the box containing the detection.
4. Divide by the area of the detection to normalize for size.
5. Normalize this value by the maximum possible response of the kernel.

In step 1, the box to be extracted from the image must be large enough to contain the entire detection and the kernel on each side. This technique ensures that the information about the border is not lost. Step 5 is a technique developed for this thesis. Since these features are being used in a classifier, the maximum and minimum responses to the kernels need to be known for feature vector normalization. The l5l5 kernel is the only kernel which does not sum to zero. The maximum response to this kernel is achieved when the 5x5 kernel is positioned over a 5x5 block of pixels inside the detection all with the value of 4095, the maximum intensity using 12 bits. This maximum, as well as the maximums for the other 24 kernels, are shown in Table 6. The minimum for all kernels is zero.

Since the other 24 kernels have both positive and negative values, which sum to zero, the maximum response occurs under two circumstances: 1) all positive cells are positioned over pixels with values of 4095 and all negative cells are positioned over zeros, or 2) since the absolute value is taken in step 3, the opposite of the first case occurs and negatives lie over 4095 pixels and positives lie over zeros. Although these circumstances have extremely low probabilities, this technique allows all features to be within a given range in proximity to the scale of other features. The importance of this is that the classifier can be trained using normalized training data without difficulties when testing with samples that could results in much greater values.

Feature extraction is now complete. The mask of possible tumors that entered this module has now been transformed into vectors containing information about the shape and texture of each detection. Having extracted these 34 features from each of the suspect regions, a classifier is used to differentiate between masses and normal tissue to reduce the number of false positive detections.

3.3.7.2 Classifier. Through experimentation, an artificial neural network (ANN) was selected as the classifier for the mass detection system. Background on ANNs can be found elsewhere (40). This thesis will only describe its ANN configuration.

Figure 19 shows the feedforward back-propagation ANN used as the mass detection system classifier. The initial neural network had the 34 features as inputs. The number of features was later reduced through feature selection, which will be discussed in Section 4.3.3. Tangential sigmoids were experimentally selected for the activation function for the hidden and output nodes. The network produced the most favorable results using five hidden nodes. A single output node was chosen so that a threshold could be set to get specific TP and FP rates during training and then used to test.

The network was trained on 10 different sets of 45 true mass samples and 45 samples of false alarms. A threshold was set on the outputs of the network and used to test the remaining data. Results of the ANN will be discussed in Chapter IV.

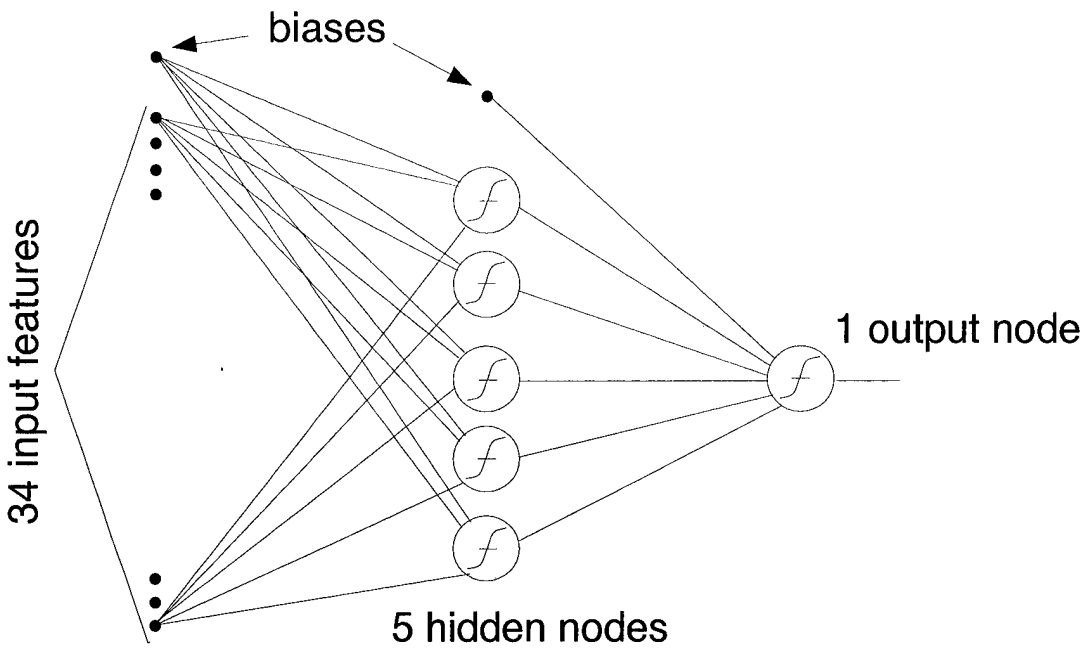

Figure 19 Multilayer Perceptron Classifier Architecture using 34 features as input and generating a single output value that is compared to a threshold for classification.

3.4 Summary

This chapter introduces the AFIT database and the methods used in the mass detection system. The database consists of 55 cases, totaling 104 images, which contain 108 masses. Size and contrast of each mass was calculated and presented. When compared to other databases, the AFIT database contains the largest percentage of small, low contrast masses. The mass detection system was discussed by detailing each of its components. Various options, such as different preprocessing, were discussed. Experimetnal results will be discussed in Chapter IV

IV. Results and Analysis

4.1 Introduction

This chapter explains the conditions of evaluating the mass detection system, the selection of parameters, and the performance of the system on the AFIT database.

4.2 Evaluating Results

The mass detection system was designed using a database of 104 images containing a total of 108 masses. As Nishikawa showed, system performance can be drastically skewed based on choice of database (35). Since the database contains low contrast masses of a variety of sizes and not simply a small set of easy cases, the detection portion of the system is designed using the entire 108 masses. Due to the diverse content of the database, using the entire database is the best means of setting parameters for the DOG filter and PCNN. However, for feature selection and classifier design, 10 separate training sets of 45 TPs and 45 FPs are used to allow for good generalization of the classifier.

The goal of the thesis is to detect masses while maintaining a practical false detection rate. The approach is to first detect as many masses as possible and, then to reduce the number of false detections without significantly lowering the number of true positives detected.

A mass is considered detected if the mass intersects the truth box and the centroid is within 0.5 cm of the truth box. Under these conditions, the results would aid the radiologist by drawing attention to the location of the mass.

4.2.1 Parameter Selection. Parameter selection and system design are performed using two means of analysis. 1) A genetic algorithm (GA) is used to find a range of good parameters. 2) Free-response receiver operating characteristic (FROC) analysis is used to evaluate system performance using specific parameters.

4.2.1.1 Genetic Algorithm. A GA is an adaptive search procedure based on genetic search techniques, such as mutation and sexual recombination (18). For more details on GAs and function optimization see (18, 36). For this thesis, the GA performs

function optimization to find the optimal combination of DOG filter size and PCNN settings to detect masses. The optimization function is designed to obtain as many TPs as possible with a reasonable number of FPs.

4.2.1.2 FROC Analysis. The FROC curve is the tool used to graphically report the performance of CAD systems (32). The FROC curve relates the trade-off of TP fraction to the number of FPs per image. Results may be reported as a point on the curve or by the area under the curve. In this thesis, FROC analysis is used to make decisions on parameter settings.

4.2.1.3 Combining Techniques. Due to the size of the database and the time to process each mammogram, a combination of search techniques is needed to find the optimal parameters for the system. The system is first designed and functionality proven by experimenting with parameters. Next the GA is assigned a optimization function to minimize. Since it takes the GA several hours to evaluate a single point in the search space. The results of the GA are used to seed further experimentation in a particular range of parameter settings. When a low fitness value is returned by the GA, independent experimentation is performed in the immediate area of the settings the GA used to obtain the fitness. Once a large enough range of settings have been analyzed, a FROC is developed to further compare parameter settings.

4.3 Component Results

The results of the system can be tracked by its performance at different locations which are component and parameter dependent. Analysis will be presented on the effects of the following on the performance of the system: 1) preprocessor selection, 2) choice of DOG filter and PCNN parameters, 3) selection of features and 4) design of the neural network for classification. These points can be found in Figure 20.

4.3.1 Preprocessor Module. The performance of the system using different preprocessing modules is best analyzed using Table 7. While fixing the DOG filter and PCNN module parameters, each preprocessor is inserted into the system. Although results could

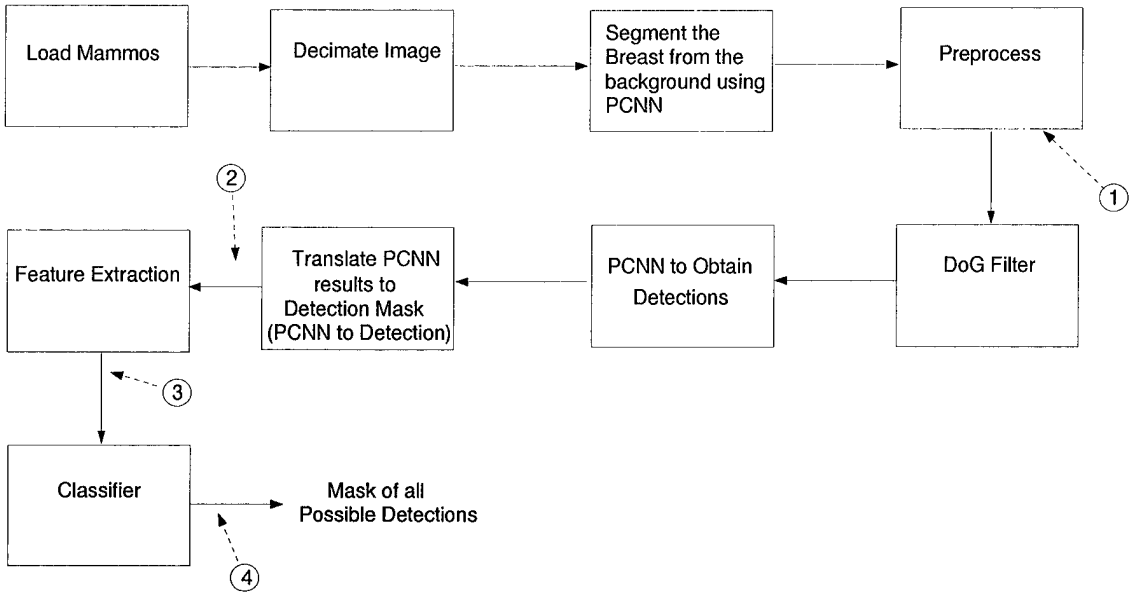

Figure 20 Mass Detection System using a Difference of Gaussians filter and Pulse Coupled Neural Network. The labels indicate points where decisions and results will be discussed.

Table 7 Performance of the System at the output of the PCNN to Detection Mask stage as effected by using different preprocessors. The results are based on 104 images containing 108 TPs. The following parameters were fixed: dogsize = 25, beta = .35, timesteps = 50.

	TPs	FPs
No Preprocessor	79	642
Histogram Equalization	83	926
Mean Background	89	824
Mirror-padding the Breast Edge	63	499

vary slightly with different parameter settings, the mean background is chosen as the preprocessor since it detects the largest number of TPs under these set conditions. This preprocessor is used to obtain the remaining results in this chapter.

4.3.2 PCNN to Detection Mask Module. The performance of the system is first calculated at the output of the PCNN to Detection Mask module and later at the output of the neural network (points 2 and 4, respectively, in Figure 20. Parameters for the DOG filter and PCNN modules are set based on FROC analysis. The results of several DOG filters are processed by the PCNN with varying linking strength, β, to find the combination

Table 8 Per case results of the system at the output of the PCNN to Detection module for the database of 55 cases. The following parameters are used to achieve these results: dogsize = 19, beta = .39375, timesteps = 50. On an individual basis, this translates to 96 detections out of 108 possible masses.

	4-view	2-view	1-view
# detected	1	45	7
# possible	1	46	8
%	100	97.83	87.50

to maximize the number of detections. Figure 21 is a FROC curve to analyze the settings for these stages. The parameters are chosen as those which generated the highest curve peak, the highest TP fraction. The DOG filter to achieve this point has a distance between zero crossings of 19. This size DOG filter is able to detect a broad size range of masses. The choice of the β is important to the DOG size selection. A larger β will permit the use of a smaller DOG filter and vice versa, since the number of pixels pulsing at one time will effect the size of the detection and whether it is too large or small to remain in consideration as a mass. A β of .39375 achieved the highest TP fraction with a DOG filter size of 19. The results of the entire database at the output of the PCNN to Detection stage using these settings are shown in Table 8. Complete results for each mass is found in Appendix A.

4.3.3 Feature Selection. A problem, frequently encountered when designing a classifier, is the "curse of dimensionality" whereby designing a good classifier becomes rapidly more difficult as the dimensionality of the input space increases (4). One way of dealing with this problem is to reduce this dimensionality prior to designing the classifier. This is done through feature selection.

The mass detection system began with 34 features as shown in Table 9. The classifier is trained using 45 TP and 45 FP samples. According to Foley (12), $3n$ feature vectors should be used for each class. To maintain this boundary, the number of features would need to be reduced to 15. The Foley criteria is actually a lower bound and the number of features should be reduced even further (41). For this reason, the dimensionality of features is reduced from 34 to 10 through feature selection. This reduction should improve accuracy, reduce computations, and allow a classifier which will generalize to be designed.

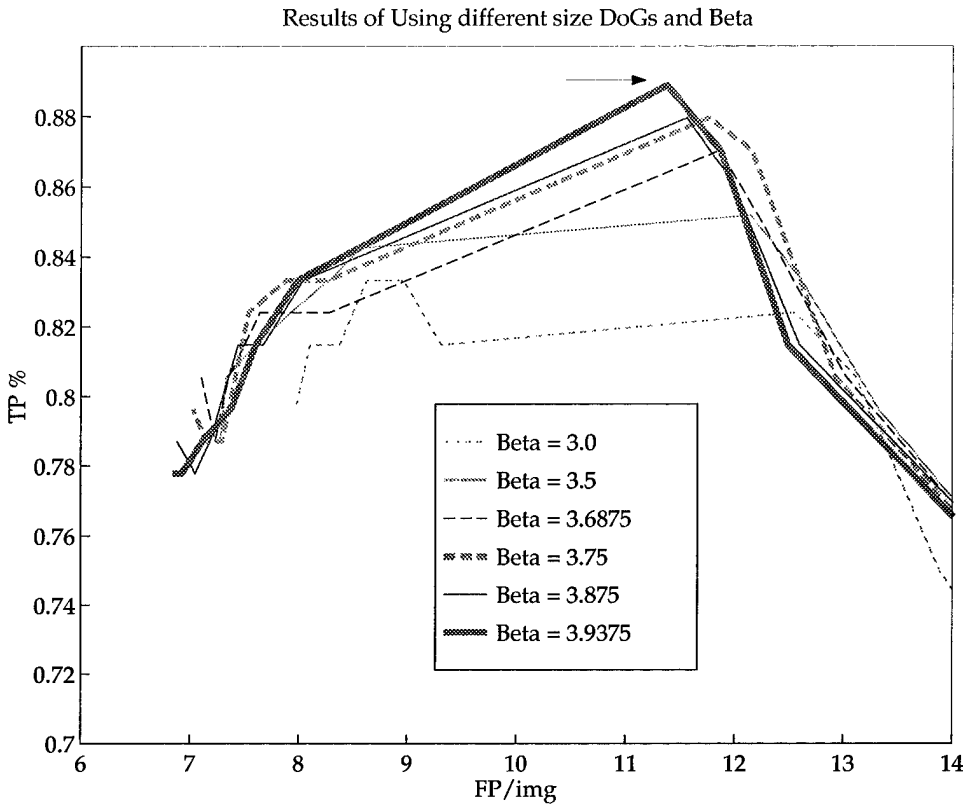

Figure 21 The parameters for the DOG and PCNN modules are chosen based on their performance. The curves are created by fixing the β and varying the dogsize from 31 to 11 from left to right on the curves. The arrow points to desired location. The following parameters were used to achieve this point: $dogsize = 19$ and $\beta = .39375$.

Table 9 The 34 features to be reduced. Features 9 through 33 represent the 5x5 Laws kernel name.

Number	Feature	Number	Feature	Number	Feature	Number	Feature
1	Circularity	10	E5S5	19	L5W5	28	E5R5
2	Rectangularity	11	L5S5	20	S5L5	29	E5E5
3	Min Distance	12	L5E5	21	S5R5	30	W5L5
4	Compactness	13	W5R5	22	S5W5	31	W5W5
5	Mean NRL	14	S5S5	23	R5S5	32	W5E5
6	Standard Dev NRL	15	S5E5	24	R5L5	33	W5S5
7	Area Ratio NRL	16	E5W5	25	R5E5	34	Area
8	ZCC NRL	17	L5L5	26	R5W5		
9	R5R5	18	L5R5	27	E5L5		

Three techniques, Fisher Ratio, Forward Selection, and Cascade Correlation, are used to evaluate ability of features to discriminate and level of correlation between features. Each technique is evaluated over ten separate datasets consisting of 45 TPs and 45 FPs.

1. Fisher Ratio

   The Fisher Ratio (F-ratio) is defined as (4)

$$\text{F-ratio} \equiv \frac{\text{variance of the means (over all classes)}}{\text{mean of the variances (within-classes)}}, \tag{13}$$

   or for two classes

$$\text{F-ratio} \equiv \frac{(\mu_1 - \mu_2)^2}{\sigma_1^2 + \sigma_2^2}, \tag{14}$$

   where μ_1 and μ_2 are the class means and σ_1 and σ_2 are the standard deviations for classes 1 and 2 respectively.

2. Forward Selection

   Forward feature selection iteratively finds the best combination of features which achieve the best classification accuracy. Forward feature selection first finds the one feature which best classifies the data. The next feature found is the one that performs the best as a pair when grouped with the first feature. This process continues until all features have been added. One example of this process is shown in Figure 22.

3. Cascade Correlation

   Cascade correlation generates a set of uncorrelated features. This process iteratively selects the feature most correlated with class label and eliminates features which are correlated above a threshold with this feature(16). The threshold is adjusted until the desired number of features are eliminated. The results of this process are shown in Table 10.

After all three techniques are used on each of the ten datasets, results are calculated and features ranked based on the frequency of occurring in the top 10 and top 5 of the features. Complete results are shown in Table 11. Table 12 displays the Top 10 features of each technique. A fourth set of ten features is created by combining the top 4 features

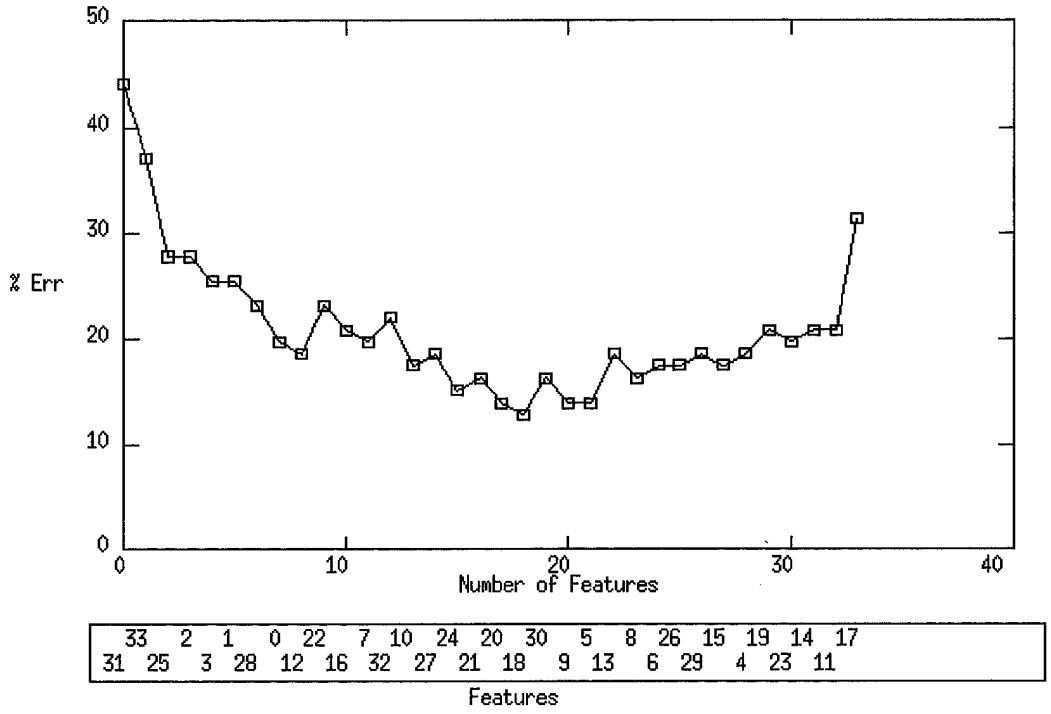

Figure 22 The results of one forward feature selection process. The feature numbering at the bottom of the graph should be incremented by 1 to translate with the feature labeling in this thesis. The features listed on the bottom are in the order as they were used to obtain the results in the graph. Thus for this set of data, feature 32 obtained the best classification accuracy alone. Note: the lowest error occurs using less than the total set.

Table 10 The results of a single trial of Cascade Correlation keeping the feature with the highest class correlation and eliminating all features correlated above .7 with it. This is done iteratively across the remaining features. The bottom 2 features were both uncorrelated with class and uncorrelated with each other.

Feature Kept	Features Eliminated
32	14,15,22,23,24,25,26,30,31,33
9	13,21
20	27
17	
28	10,16
5	1,4,6,7
29	
18	11,12
34	
8	

from the forward selection with the top 3 from the Fisher Ratio and cascade correlation techniques. This set is used to evaluate the performance of the other three sets.

For each of these four pools of features, 10 datasets of 45 TPs and 45 FPs are created. The dimensionality of each of these sets are 90x10, 90 feature vectors of 10 features each. Each dataset is used to design a classifier configuration.

4.3.4 Classifier. Classifier selection was accomplished by evaluating classifier performance over 10 iterations of data of each of the 40 datasets previously discussed. Results varied dependent both on the technique used for feature selection and the dataset being used, so results were compared over all datasets. Through experimentation, the neural network is chosen to have its 5 hidden nodes and 1 output node to have tangential sigmoidal activation functions and is trained for 100 epochs. This configuration is shown in Figure 19.

Once the configuration is set, the neural network is trained using 10 different sets of 45 TPs and 45 FPs for each feature selection technique. Figure 23 shows a FROC of the average performance of the four techniques and also using the initial 34 features. The best performance, in terms of lowest number of FPs per image while maintaining a TP fraction above .9, is obtained using the Cascade Correlation features with a threshold of .6. At lower levels of TP fractions, the method using all 34 features achieves lower FPs per

Table 11 Each technique is run on 10 different sets of training data. The shown rank-ordered features based on the number of times each appear in the Top 10/Top 5 best features for classification during the 10 iterations. 6/2 as seen for feature 1 indicates that this features was among the Top 10 features 6 out of the 10 iterations and among the Top 5 features 2 of those times. When selecting the best features, first the Top 10 frequency is examined and then the Top 5 frequency if features appeared in the Top 10 the same amount of times.

	Fisher Ratio		Forward Selection		Cascade Correlation	
Feature	Top 10	Top 5	Top 10	Top 5	Top 10	Top 5
1	2	1	4	1	0	0
2	1	0	2	0	4	0
3	1	1	4	2	9	3
4	2	2	3	2	2	1
5	3	3	4	3	5	2
6	4	2	4	4	2	1
7	4	3	2	2	3	2
8	0	0	0	0	10	0
9	2	0	3	2	2	2
10	4	2	5	2	0	0
11	2	1	3	1	2	1
12	1	0	1	0	2	1
13	1	0	4	2	0	0
14	3	2	3	2	0	0
15	5	2	2	1	0	0
16	3	1	5	1	0	0
17	4	1	3	1	9	6
18	1	1	3	0	2	1
19	1	1	1	1	5	3
20	3	1	4	2	5	4
21	2	1	4	1	1	1
22	4	2	3	2	2	1
23	6	3	3	1	2	0
24	3	0	5	1	2	2
25	6	4	0	0	2	2
26	5	4	3	2	3	3
27	0	0	5	3	3	1
28	2	1	3	1	3	2
29	3	1	3	2	4	2
30	5	3	1	0	2	2
31	2	0	2	1	2	1
32	8	6	3	3	2	2
33	5	1	2	2	0	0
34	2	0	3	2	10	4

Table 12 The Top 10 features of each selection technique as ranked by the number of times in the Top 10. When a tie occurs, the number of times in the Top 5 is compared. The last way to differentiate between features is the lower combined total placement, such that if a feature placed 3, 4, and 5, the score would be 12.

Rank	F-Ratio	Forward Selection	Cas. Corr
1	32	27	34
2	25	10	8
3	23	24	17
4	26	16	3
5	30	6	20
6	15	5	5
7	33	20	19
8	7	22	29
9	22	13	2
10	6	21	26

Table 13 Results of the System on the Entire Set. Final TP and Final FP are the results after the neural network. Detection TP and Detection FP are the results prior to entering the classifier. Thus the classifier misclassified 7 TPs while successfully eliminating 456 FPs. Calculations are based on 108 masses in 104 images.

	TP	TP Fraction	FP	FP/img
Detection	96	.89	1183	11.37
Final	89	.824	697	6.7

image rates. However, at point greater than a TP fraction of .9, the Cascade Correlation techniques provides the best results.

Once the entire neural network is configured, the 104 images of the database are processed through the entire system. The results of the system are found in Table 13.

4.4 Analysis of Results

The complete results of each of the 108 masses are shown in Appendix A. The final results of the system on a per image basis are 82.4% detection of TPs with 6.70 FP per image. 12 masses were never detected. Possible reasons for this are that the masses were too small or large, completely hidden in its background tissue, or something remained on the digitized image, which did not allow the film to be processed correctly.

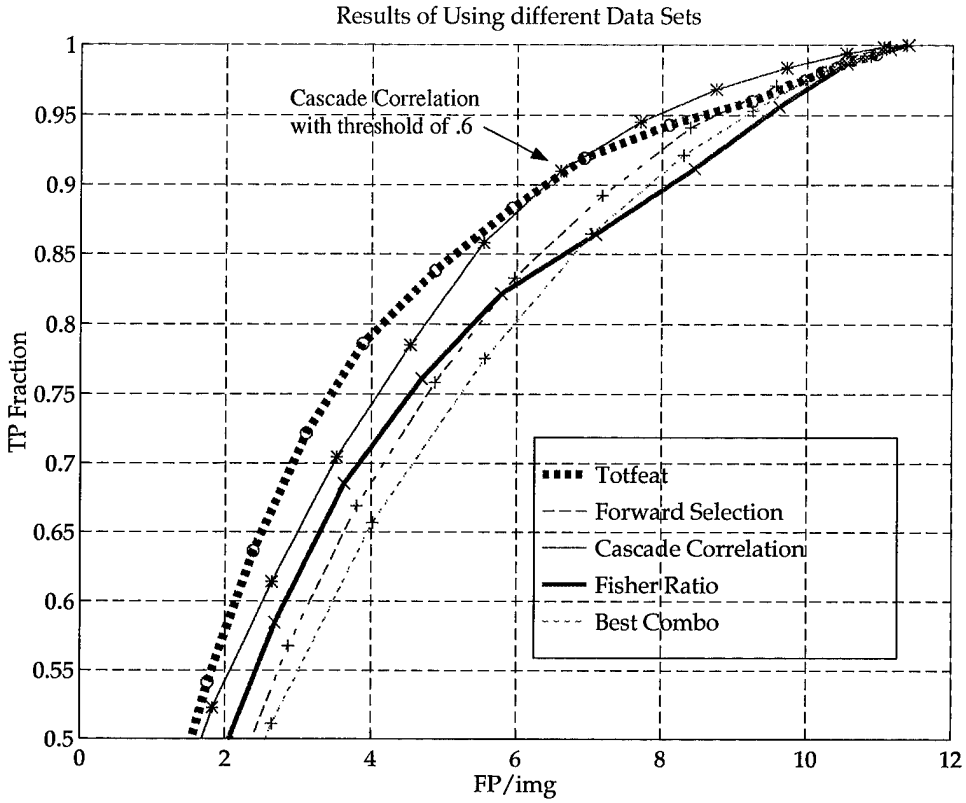

Figure 23 The results of using 5 different techniques to train a neural network to classify masses from FPs. Each technique is the average performance of the network over 10 different sets of training data. Totfeat is the results of the network using a training set of 90 vectors (45 TPs and 45 FPs) with all 34 features. The other four techniques are those discussed in Section 4.3.3. The o,x, etc. represent the different thresholds that can be set to obtain the indicated results. The arrow points to the lowest FP fraction possible while maintaining a TP fraction of greater than .9. This point is achieved with the Cascade Correlation features and a threshold on the outputs of the neural network of 0.6. Note: the y-axis is based on percent of masses retained by the classifier.

Table 14 These results are based on the performance of the system on a per case basis. If the mass was detected in one view, then the case is considered to be detected.

	# Cases	# PCNN Detected	%	# NN Detected	%
4-view	1	1	100	1	100
2-view	46	45	97.83	44	95.65
1-view	8	7	87.5	7	87.5
Total	55	53	96.36	52	94.55

The complete case results for the system are shown in Table 14. Based on a two view per case basis, these results translate to .9455 TP fraction with 13.4 FPs per case.

These results show that the detection scheme performs well in detecting masses in mammograms. The classifier is capable of maintaining an acceptable detection rate while eliminating 4.67 FPs per image.

4.5 Conclusion

This chapter presents how results are evaluated, how parameters are selected, and the total results of the system. The goal of this thesis is to detect masses. For this reason, parameters are selected through FROC analysis to detect as many masses as possible and then to eliminate FPs using a classifier. The final results were 1) a per case TP fraction of .9455 with 13.4 FPs and 2) a per image TP fraction of .824 with 6.7 FPs.

V. Conclusion

The aim of this research was to develop a new CAD algorithm to identify masses in mammograms to aid a radiologist in making decisions. This chapter explains how this goal was accomplished through the development of a mass detection system using a Difference of Gaussian (DOG) filter and a Pulse Coupled Neural Network (PCNN). The contributions of this research and recommendation for future work are also addressed.

5.1 Contributions

This research made the following contributions to AFIT and the field of CAD research:

1. Completely characterized the AFIT database for easy comparison to other databases.
2. Designed a new mass detection algorithm using a PCNN.
3. Created self-normalized Laws texture features.

5.2 Conclusions and Recommendations

The mass detection system performed well in detecting masses in digitized mammograms. On a per case basis, the system detects 96.36 percent (54 of 55 cases) of masses. Its per image detection rate is 89 percent (96 of 108 masses). However, this high TP rate results in a high FP per image rate as well. Therefore, a classifier is used to lower the number of FPs per image while attempting to maintain an adequate TP fraction. The classifier retained 92.78 percent of the TPs it received and successfully eliminated 456 FPs. Therefore, the final results on a per image basis were a TP fraction of .824 with 6.7 FPs per image and on a per case basis, were a TP fraction of .9455 with 13.4 FPs per case.

These results show that the Difference of Gaussians filter is capable of detecting a wide range of masses. Possible work in this area would be to use multiple DOG filters and fuse their outputs, such that the number of FPs per image does not multiply. The PCNN proved to be a good tool for both segmenting the breast from background and detecting masses in the DOG filter output. Future use for the PCNN include using it to 1) detect

masses from the original image, 2) obtain better features of ROIs, and 3) adaptively set itself over the entire database to perform best in the mass detection system. The classifier results show that work remains in discriminating between TPs and FPs. Among the ways this can be accomplished is through creating better features or better detections from which to calculate features. Ultimately, the best way to evaluate the success of the system is through a clinical study to develop a better understanding of how a CAD mass detection system can best aid a radiologist and, more importantly, how this mass detection system will help radiologists.

Appendix A. Mass Statistics and Results

This appendix details the characteristics of each mass as well as specifies if the mass was detected and whether it was classified correctly. Area is in terms of the number of pixels contained in the mass. Diameter is calculated as described in Chapter 3. Exterior and Interior Intensity are the mean intensities of the pixels inside and outside the mass also as described in Chapter 3. Contrast is the difference of the mean intensities divided by the sum of the mean intensities. Difference in OD is the mean exterior OD subtracted from the mean interior OD. Detected is a binary indicator (1/0 = Yes/No) of whether the mass was detected at the output of the PCNN to Detection module. Classified is a binary indicator (1/0 = Yes/No) whether the mass was retained by the neural network.

Name	Area (# pixels)	Equivalent Diameter (mm)	Exterior OD	Interior OD	Contrast	OD Difference	Detected	Classified
a001d00m	1215	39.33	2.4281	2.6518	0.0440	0.2237	1	1
a002b00m	14642	136.54	2.8452	3.2513	0.0666	0.4062	1	1
a002d00m	18664	154.15	3.4630	3.5657	0.0146	0.1027	0	0
a003a00m	2697	58.6	2.5440	3.0297	0.0871	0.4856	1	1
a003c00m	8430	103.6	2.8144	3.2939	0.0785	0.4795	1	1
a004b00m	11032	118.52	2.5608	3.1882	0.1091	0.6274	1	1
a004d00m	11211	119.48	2.7993	3.0311	0.0398	0.2318	1	1
a005b00m	9107	107.68	2.1267	2.3124	0.0418	0.1857	1	0
a005d00m	6720	92.5	2.4334	2.7936	0.0689	0.3602	1	1
a007a00b	16045	142.93	2.4945	3.2259	0.1278	0.7313	1	1
a007c00b	14792	137.24	2.8729	3.2304	0.0586	0.3575	1	1
a008b00b	14200	134.46	2.4168	2.9020	0.0912	0.4853	1	1
a008d00b	9838	111.92	2.6506	3.0574	0.0713	0.4069	1	1
a009a00m	2996	61.76	2.4868	2.8381	0.0660	0.3513	1	1
a009c00m	5885	86.56	2.7965	3.2288	0.0717	0.4323	1	1
a011b00m	9438	109.62	2.6610	2.9346	0.0489	0.2735	1	1
a011d00m	9321	108.94	2.7145	2.9402	0.0399	0.2258	1	0
a012b00b	3525	66.99	2.7890	2.9639	0.0304	0.1749	1	1
a012d00b	3465	66.42	2.8505	3.0323	0.0309	0.1818	0	0
a013b00b	3766	69.25	2.4941	2.6786	0.0357	0.1845	1	1
a015a00m	7221	95.89	2.2179	2.6439	0.0876	0.4260	1	1
a015c00m	11113	118.95	2.7394	3.1390	0.0680	0.3996	1	1
a017b00b	22574	169.53	3.0489	3.3135	0.0416	0.2646	1	1
a017d00b	13936	133.21	2.8534	3.1831	0.0546	0.3297	1	1
a018a00m	4771	77.94	3.4062	3.5334	0.0183	0.1273	1	1
a018c00m	3749	69.09	2.3486	2.6808	0.0661	0.3322	1	1
a019a00b	9325	108.96	2.4473	2.6504	0.0399	0.2032	1	1
a019c00b	7059	94.80	2.6925	2.9102	0.0389	0.2177	1	1
a020b00	9691	111.08	1.9530	2.3474	0.0917	0.3944	1	1
a020d00b	1274	40.28	1.8459	2.0891	0.0618	0.2432	0	0
a021a00m	3755	69.14	2.7000	2.9914	0.0512	0.2914	1	1
a021c00m	5549	84.05	2.6697	2.9438	0.0488	0.2741	1	1
a022a00m	1779	47.59	2.7154	2.8831	0.0300	0.1677	0	0
a022c00m	3880	70.29	2.3995	2.5852	0.0373	0.1857	1	1
a023a00b	6352	89.93	2.8718	3.1502	0.0462	0.2785	1	1
a023c00b	9543	110.23	2.2120	2.6861	0.0968	0.4741	1	1

Name	Area (# pixels)	Equivalent Diameter (mm)	Exterior OD	Interior OD	Contrast	OD Difference	Detected	Classified
a025a00b	0.4221	0.7331	2.2661	2.4863	0.0463	0.2203	1	1
a025a00b	0.1917	0.4940	2.7769	3.0026	0.0390	0.2257	1	1
a025c00b	0.3387	0.6567	2.3664	2.5711	0.0415	0.2047	1	1
a025c00b	0.4859	0.7866	2.3692	2.5921	0.0449	0.2229	1	1
a027b00m	0.4765	0.7789	2.8469	3.0987	0.0424	0.2518	1	1
a027d00m	0.6309	0.8963	2.7506	2.9919	0.0420	0.2413	1	1
a028d00m	0.4264	0.7368	2.5344	2.7747	0.0453	0.2403	1	1
a030b00b	2.9332	1.9325	2.9127	3.2471	0.0543	0.3345	1	1
a030d00b	2.3664	1.7358	2.3833	2.9798	0.1112	0.5965	1	1
a031a00b	1.0527	1.1577	2.4664	2.7687	0.0577	0.3023	1	1
a031c00b	1.2282	1.2505	2.0704	2.5247	0.0989	0.4544	1	1
a032a00m	0.3212	0.6395	2.7984	3.0051	0.0356	0.2067	1	1
a032c00m	0.4546	0.7608	2.5497	2.8135	0.0492	0.2638	1	1
a034b00b	3.5862	2.1368	2.5137	2.7679	0.0481	0.2543	1	1
a034d00b	2.0585	1.6189	2.6358	2.9789	0.0611	0.3431	1	1
a035a00b	3.6601	2.1587	2.5642	2.8831	0.0585	0.3189	1	1
a035c00b	2.8473	1.9040	2.9284	3.3038	0.0602	0.3754	1	1
a037b00m	0.8110	1.0162	2.5732	2.7603	0.0351	0.1871	1	1
a037b00m	1.4187	1.3440	2.5276	2.9597	0.0787	0.4320	1	1
a037d00m	3.3756	2.0731	2.5471	2.8049	0.0482	0.2577	1	1
a037d00m	2.1760	1.6645	2.7645	3.1185	0.0602	0.3540	0	0
a038a00m	0.2055	0.5115	2.8328	3.0507	0.0370	0.2178	1	1
a038c00m	0.8321	1.0293	2.6147	2.9137	0.0541	0.2990	1	1
a039a00b	0.8674	1.0509	2.8086	3.1909	0.0637	0.3823	1	1
a039c00b	0.8211	1.0225	2.6620	3.1158	0.0785	0.4538	1	1
a040a00b	1.1684	1.2197	2.7733	3.1276	0.0600	0.3542	1	1
a040c00b	1.3470	1.3096	2.1839	3.0095	0.1590	0.8256	1	1
a042a00b	1.3135	1.2932	2.5547	3.2001	0.1121	0.6454	1	1
a042c00b	1.0965	1.1816	2.4880	3.0015	0.0936	0.5135	1	1
a044b00m	0.1659	0.4596	2.1451	2.4175	0.0597	0.2724	0	0
a044d00m	0.3238	0.6421	2.2963	2.5266	0.0478	0.2303	0	0
a045a00m	0.6146	0.8846	2.8911	3.1529	0.0433	0.2618	1	1
a045c00m	0.5869	0.8644	2.7419	3.0216	0.0485	0.2797	1	1
a046b00b	1.3342	1.3034	2.9120	3.2408	0.0534	0.3288	1	1
a046d00b	0.5656	0.8486	2.8672	3.0706	0.0343	0.2034	1	0
a047b00b	1.2303	1.2516	2.8056	3.1626	0.0598	0.3569	1	1

Name	Area (# pixels)	Equivalent Diameter (mm)	Exterior OD	Interior OD	Contrast	OD Difference	Detected	Classified
a049a00m	0.3629	0.6797	2.9137	3.2422	0.0534	0.3285	1	1
a049b00m	4.3183	2.3448	2.7557	3.4857	0.1170	0.7300	1	1
a049c00m	1.3563	1.3141	2.5357	2.9324	0.0725	0.3967	1	1
a049d00m	2.0726	1.6245	2.2264	3.3476	0.2011	1.1212	1	1
a050a00m	0.3670	0.6836	2.6967	2.9179	0.0394	0.2213	1	1
a050c00m	0.6356	0.8996	2.8326	3.0185	0.0318	0.1859	1	1
a051a00b	0.5796	0.8591	2.3194	2.6419	0.0650	0.3226	1	1
a051c00b	0.5366	0.8266	2.0842	2.3364	0.0571	0.2522	1	1
a053b00m	3.5237	2.1181	2.4195	3.2902	0.1525	0.8706	1	1
a053d00m	2.1449	1.6526	2.8494	3.3832	0.0856	0.5337	1	1
a054b00m	1.8811	1.5476	2.0735	2.5519	0.1034	0.4784	1	1
a054d00m	4.1078	2.2870	2.5627	3.1746	0.1067	0.6119	1	1
a055a00b	0.2546	0.5694	2.5667	2.8553	0.0532	0.2886	1	1
a055c00b	0.7672	0.9883	1.9155	2.5230	0.1369	0.6075	1	0
a056a00b	0.4039	0.7171	2.2168	2.5290	0.0658	0.3123	1	1
a059b00b	0.5316	0.8227	2.5572	2.8859	0.0604	0.3288	1	1
a059d00b	0.4478	0.7551	0.9849	1.3177	0.1445	0.3328	0	0
a061a00b	0.6737	0.9262	2.4970	2.7735	0.0525	0.2765	1	1
a061c00b	0.5389	0.8283	2.3646	2.5813	0.0438	0.2167	1	0
a063a00m	0.7104	0.9511	1.8387	2.0920	0.0645	0.2534	1	0
a063c00m	0.2776	0.5945	2.1236	2.4336	0.0680	0.3100	1	0
a064b00m	0.4122	0.7245	1.3781	1.8097	0.1354	0.4316	0	0
a064d00m	0.3318	0.6500	2.1533	2.5446	0.0833	0.3913	1	1
a065b00b	0.3378	0.6558	2.0744	2.5921	0.1109	0.5176	1	1
a065d00b	0.4335	0.7429	2.7247	2.9899	0.0464	0.2653	0	0
a066b00b	2.0936	1.6327	2.9968	3.1455	0.0242	0.1487	1	1
a066d00b	1.6551	1.4517	2.9139	3.0946	0.0301	0.1808	0	0
a070c00b	0.4420	0.7502	1.9839	2.4014	0.0952	0.4175	0	0
a071b00b	0.1792	0.4777	1.9125	2.2938	0.0907	0.3813	1	1
a071d00b	0.4374	0.7463	2.1009	2.5227	0.0912	0.4217	1	1
a072b00m	0.6768	0.9283	2.6086	3.1612	0.0958	0.5527	1	1
a072d00m	1.0128	1.1356	2.3157	2.9055	0.1130	0.5898	1	1
a074a00m	1.2648	1.2690	2.3232	2.7246	0.0795	0.4014	1	1
a074c00m	0.8806	1.0589	2.3008	2.7333	0.0859	0.4326	1	1
a075c00m	7.0754	3.0014	1.9458	2.4741	0.1195	0.5283	1	1
a076c00m	7.0852	3.0035	2.9149	3.4609	0.0856	0.5460	1	1

Bibliography

1. Abrahamson, Shane. "Segmenting magnetic resonance brain images using pulse coupled neural networks," *Submitted to IEEE TMI* (January 97).

2. Bird, R. E. "Professional quality assurance for mammography screening programs," *Radiology*, *177*(2):587 (1990).

3. Bird, R. E., et al. "Analysis of cancers missed at screening mammogrpahy," *Radiology*, *184*:613–613 (1992).

4. Bishop, C. M. *Neural Networks for Pattern Recognition*. New York: Oxford University Press, 1995.

5. Broussard, Randy. *Physiologically based vision modelling applications and gradient descent based parameter adaption of pulse coupled neural networks*. PhD dissertation, AFIT, 1997.

6. Broussard, Randy. "Physiologically motivated image fusion for object detection using a pulse coupled neural network," *Accepted for publication in IEEE Transactions on Neural Networks* (1997).

7. Cardenosa, G. and G. W. Eklund. "Breast anatomy, histology, and cancer," *RSNA Categorical Course in Breast Imaging*, 21–28 (1995).

8. Chan, H.-P, et al. "Computer-aided classification of mammographic masses and normal tissue: linear discriminant analysis in texture feature space," *Phys. Med. Biol.*, *40*:857–876 (1995).

9. Chang, Y.-H., et al. "Robustness of computerized identification of masses in digitized mammograms," *Investigative Radiology*, *31*(9):563–568 (1996).

10. Dauk, R. *Computer-aided detection of microcalcifications using texture analysis*. MS thesis, AFIT, 1995.

11. Eckhorn, R., et al. "Feature linking via synchronization among distributed assemblies: simulations of results from cat visual cortex," *Neural Computation*, 293–307 (1990).

12. Foley, D. "Consideration of Sample and Feature Size," *IEEE IT*, *18*(5):618–626 (September 1972).

13. Giger, M. L. "Computer-aided diagnosis," *RSNA Categorical Course in Physics*, 287–302 (1994).

14. Giger, M. L. and H. MacMahon. "Image processing and computer-aided diagnosis," *Radiologic Clinics of North America*, *34*(3):565–596 (May 1996).

15. Gonzalez, R. C. and R. E. Woods. *Digital Image Processing*. Reading, MA: Addison-Wesley, 1992.

16. Gregg, D. W. *Decision Boundary Analysis Feature Selection for Breast Cancer Diagnosis*. MS thesis, AFIT, March 1997.

17. Hoffmeister, Dr Jeffrey. "Personal Interviews." Performed truthing of database, 1996-97.

18. Holland, J. "Genetic Algorithms," *Scientific American*, 66 – 72 (July 1992).

19. Huo, Z., et al. "Analysis of spiculation in the computerized classification of mammographic masses," *Medical Physics*, *22*(10):1569–1579 (October 1995).

20. Kaewlium, A. and H. Longbotham. "Application of Gabor transform as texture discriminator of masses in digital mammograms," *DISA Paper 93-023* (1993).

21. Karssemeijer, N. and Guido M. te Brake. "Detection of stellate distortions in mammograms," *IEEE TMI*, *15*(5):611–619 (October 1996).

22. Kegelmeyer, W. "Evaluation of stellate lesion detection in a standard mammogram data set," *International Journal of Pattern Recognition and Artificial Intelligence*, *7*(6):1477–1492 (December 1993).

23. Kegelmeyer, W. P., et al. "Computer-aided mammographic screening for spiculated lesions," *Radiology*, *191*(2):331–337 (1994).

24. Kilday, J., et al. "Classifying mammographic lesions using computerized image analysis," *IEEE TMI*, *12*(4):664–669 (December 1993).

25. Kocur, C., et al. "Neural network wavelet feature selection for breast cancer diagnosis," *IEEE Engineering in Medicine and Biology*, 95–102,108 (June 1996).

26. Kopans, D. B. "The etiology of breast cnacer," *RSNA Categorical Course in Breast Imaging*, 29–37 (1995).

27. Lai, S.-M., et al. "On techniques for detecting circumscribed masses in mammograms," *IEEE TMI*, *8*(4):377–387 (December 1989).

28. Laws, K. I. *Textured Image Segmentation.* PhD Dissertation, University of Southern California, January 1980.

29. Li, H. D., et al. "Markov Random Field for Tumor Detection in Digital Mammography," *IEEE TMI*, *14*(3):565–576 (September 1995).

30. Marr, D. *Vision.* San Francisco: W.H. Freeman, 1982.

31. McCandless, D. *Detection of clustered microcalcifications using wavelets.* MS thesis, AFIT, 1995.

32. Metz, C. "ROC Methodology in Radiologic Imaging," *Investigative Radiology*, *21*:720–733 (September 1986).

33. Morrow, W., et al. "Region-based contrast enhancement of mammograms," *IEEE TMI*, *11*(3):392–406 (September 1992).

34. Ng, S. L. and W. F. Bischof. "Automated detection and classification of breast tumors," *Computer and Bimedical Research*, *25*:218–237 (1992).

35. Nishikawa, R. M. and M. L. Giger. "Effect of case selection on the performance of computer-aided detection schemes," *Medical Physics*, *21*(2):265–269 (February 1994).

36. Ochoa, Edward. *Clustered microcalcification detection using optimized difference of gaussians*. MS thesis, AFIT, 1996.

37. Petrick, N., et al. "An adaptive density-weighted contrast enhancement filter for mammographic breast mass detection," *IEEE TMI*, *15*(1):59–67 (February 1996).

38. Pohlman, S., et al. "Quantitative classification of breast tumors in digitized mammograms," *Medical Physics*, *23*(8):1337–1345 (August 1996).

39. Polakowski, W., Cournoyer, D., et al. "Computer-Aided Breast Cancer Detection Diagnosis of Masses Using Difference of Gaussians and Derivative-Based Feature Saliency," *IEEE Transactions on Medical Imaging* (December 1997).

40. Rogers, S. K. and M. Kabrisky. *An Introduction to Biological and Artificial Neural Networks for Pattern Recognition*. Bellingham, Washington: SPIE Optical Engineering Press, 1991.

41. Rogers, S. K. and D. W. Ruck. "Feature Selection for Pattern Recognition Using Multilayer Perceptrons." *The Industrial Electronics Handbook*. Innodata Publishing Services, 1996.

42. Sahiner, B., et al. "Classification of Mass and Normal Breast Tissue: A Convolution Neural Network Classifier with Spatial Domain and Texture Images," *IEEE TMI*, *15*(5):598–610 (October 1996).

43. Shen, L., et al. "Application of shape analysis to mammographic calcifications," *IEEE TMI*, *13*(2):263–274 (June 1994).

44. Smith, R. A. "The epidemiology of breast cancer," *RSNA Categorical Course in Breast Imaging*, 7 – 20 (1995).

45. Society, American Cancer, "Can breast cancer be found early?." www.cancer.org.

46. Society, American Cancer, "What are the key statistics about breast cancer." www.cancer.org.

47. Tahoces, P. G., et al. "Computer-assisted diagnosis: the classification of mammographic breast parenchymal patterns," *Phys. Med. Biol.*, *40*:103–117 (1995).

48. Thurfjell, E. L., et al. "Benefit of independent double reading in a population-based mammography screening program," *Radiology*, *191*:241–244 (1994).

49. Wolfe, J. N. "Breast patterns as an index of risk for developing breast cancer," *AJR*, *126*:1130–1139 (1976).

50. Yin, F.-F., et al. "Computerized detection of masses in digital mammograms: investigation of feature-analysis techniques," *Journal of Digital Imaging*, *7*(1):18–26 (February 1994).

51. Zheng, B., et al. "Computerized detection of masses from digital mammograms: comparison of single-image segmentation and bilateral-image subtraction," *Academic Radiology*, *2*:1056–1061 (1995).

52. Zheng, B., et al. "On the reporting of mass contrast in CAD research," *Medical Physics*, *23*(12):2007–2009 (December 1996).

Vita

Lieutenant Donald A. Cournoyer was born in [redacted]. He graduated from Portsmouth Senior High School, Portsmouth, New Hampshire in June 1990. He attended Worcester Polytechnic Institute, Worcester, Massachusetts, from 1990 to 1994 earning the Bachelor of Science in Electrical Engineering degree. Upon graduation, he was commissioned in the United States Air Force. His first assignment was as a C4I Architect at the Air Force Command, Control, Communications and Computer Agency (AFC4A) at Scott Air Force Base, Illinois. In May 1996, Lieutenant Cournoyer entered the Electrical Engineering program at the Air Force Institute of Technology, specializing in communications and pattern recognition. Beginning in Dec 1997, he may be reached at the Air Force Research Laboratory in Rome, New York, working in Satellite Communications.

Permanent address: [redacted]

REPORT DOCUMENTATION PAGE

Form Approved
OMB No. 0704-0188

1. AGENCY USE ONLY (Leave blank)	2. REPORT DATE	3. REPORT TYPE AND DATES COVERED
	December 1997	Master's Thesis

4. TITLE AND SUBTITLE
Breast Cancer Mass Detection Using Difference of Gaussians and Pulse Coupled Neural Networks

5. FUNDING NUMBERS

6. AUTHOR(S)
Donald A. Cournoyer, First Lieutenant, USAF

7. PERFORMING ORGANIZATION NAME(S) AND ADDRESS(ES)
Air Force Institute of Technology, WPAFB OH 45433-6583

8. PERFORMING ORGANIZATION REPORT NUMBER
AFIT/GE/ENG/97D-07

9. SPONSORING / MONITORING AGENCY NAME(S) AND ADDRESS(ES)
Maj. Jeffrey Hoffmeister, MD
AL/CFHV Bldg 248A, 2255 H Street, WPAFB, OH 45433-7022

10. SPONSORING / MONITORING AGENCY REPORT NUMBER

11. SUPPLEMENTARY NOTES

12a. DISTRIBUTION / AVAILABILITY STATEMENT
Distribution Unlimited

12b. DISTRIBUTION CODE

13. ABSTRACT *(Maximum 200 words)*

Breast cancer will kill an estimated 43,900 women in the United States in 1997. Another 180,200 women will be newly diagnosed with breast cancer in 1997. Mammography is currently the best method for detecting breast cancer. However, a significant portion, 10 to 30 percent, of women with breast cancer have negative mammograms. Two-thirds of these false-negative mammograms prove to be evident in retrospect. Having a second radiologist perform a second reading has proven to be successful at correctly diagnosing breast cancer. A lower cost and more reliable alternative is a computer system to perform the second reading. One indicator of breast cancer is a mass or density. This research develops a new algorithm to identify masses in mammograms. The mass detection system consists of several modules. The digitized mammogram is decimated to a 512 x 256 image, preprocessed for easier detection, and filtered with a Difference of Gaussians filter. The system then detects objects with mass characteristics using a Pulse Coupled Neural Network, extracts morphological and textural features from each possible detection, and classifies as mass or normal tissue. The detection module of the system detects 89 percent of the 108 masses, 96.36 percent of the cases, with a FP rate of 11.37 per image. The classifier eliminates 4.67 FPs per image while retaining 92.7 percent of the detected masses. On a 2-view per case basis, the system successfully detects and classifies 94.55 percent of masses with 13.4 FPs per case.

14. SUBJECT TERMS
Pattern Recognition, Medical Imaging, Neural Networks, Difference of Gaussians

15. NUMBER OF PAGES
76

16. PRICE CODE

17. SECURITY CLASSIFICATION OF REPORT	18. SECURITY CLASSIFICATION OF THIS PAGE	19. SECURITY CLASSIFICATION OF ABSTRACT	20. LIMITATION OF ABSTRACT
UNCLASSIFIED	UNCLASSIFIED	UNCLASSIFIED	UL